Contents lists available at GrowingScience

Journal of Future Sustainability

homepage: www.GrowingScience.com/jfs

# Nature inspired firefighter assistant by unmanned aerial vehicle (UAV) data

**Seyed Muhammad Hossein Mousavi[a*] and Atiye Ilanloo[b]**

[a]*Developer at Pars AI Company, Tehran, Iran*
[b]*Faculty of Humanities- Psychology, Islamic Azad University of Rasht, Gilan, Iran*

**C H R O N I C L E**

*Article history*:
Received: October 10, 2022
Received in revised format: October 28, 2022
Accepted: January 18, 2023
Available online:
January 19, 2023

*Keywords:*
*Unmanned Aerial Vehicle (UAV)*
*Forest Fire Detection*
*Nature Inspired Image Processing*
*Image Segmentation*
*Classification*

**A B S T R A C T**

One of the most hazardous phenomena in forests is wildfire or bush fire and early detection of massive damage prevention is vital. Employing Unmanned Aerial Vehicles (UAV) as a visual and extinguisher tool in order to prevent this tragedy which brings fatal effects on humans and wildlife has high importance. Additionally, using aerial imagery could assist firefighters to recognize fire intensity and localize and route the fire in the forest which shrinks down casualties of firefighters. All these benefits and more is just possible by employing cheap UAVs. The proposed research uses nature-inspired image processing techniques in order to segment and classify fire in color and thermal images. Multiple nature-inspired and traditional computer vision techniques, including Chicken Swarm Algorithm (CSA) intensity adjustment (contrast enhancement), Denoising Convolutional Neural Network (DnCNN), Local Phase Quantization (LPQ) feature extraction, Bees Image Segmentation, Biogeography-Based Optimization (BBO) feature selection, Firefly Algorithm (FA) classification and more are employed to achieve high classification and segmentation accuracy. The system evaluates nine performance metrics including, F-Score, Accuracy, and Jaccard for the segmentation stage and four performance metrics for the classification stage. All experiments are conducted on the two most recent UAV fire datasets of FLAME (2021) and DeepFire (2022). Additionally, fire intensity, fire direction, and fire geometrical calculation are calculated which assists firefighters even more. As smoke shows the location of the fire, a smoke detection workflow is proposed, too. Proposed system Compared with traditional and novel methods for segmentation and classification leading to satisfactory and promising results for almost all metrics. The trained model of this system could be used in most of the current rescue UAVs in real-time applications. For the FLAME dataset (color data), segmentation precision is 95.57 % and classification accuracy is 91.33 %. Also, For the DeepFire dataset segmentation precision is 91.74 % and classification accuracy is 96.88 %.



## 1. Introduction

Based on National Interagency Fire Center (NIFC) (NIFC, 2022), World Health Organization (WHO) (WHO, 2022) reports, and (Lee et al., 2017), wildfires are responsible for 10 thousand of deaths and injuries each year globally. Also, millions of hectares of forest lands are burned down which causes producing toxic air pollution and soil quality degradation. This yearly devastating phenomenon causes a high level of financial cost to fix and restore caused damages to burned lands, infrastructures, homes, and wildlife (Smoot et al., 2021). As forests and jungles are one of the most vital elements for creatures on earth by providing shelter, medicine, and food, protecting from them is essential. Forest act as a filter to keep the water clean from different chemicals and produce fresh air constantly alongside reducing global temperature which prevents polar ice to melt fast (Jolly et al., 2015; Yuan et al., 2015). The initial cause of wildfires in 50 % of cases are unknown but it mostly is caused by human activities like camping or intentional and natural phenomenon like lightning or high temperature in dry and dense bushes (Jazebi et al., 2019). Whatever the reason is, getting notified quickly or early detection from its location, intensity and direction could aid firefighters and even locals to handle the situation much better. Unmanned Aerial Vehicles (UAVs) (Valavanis et al., 2015) are a proper replacement for Manned Aerial Vehicles such as choppers or small

* Corresponding author. Tel.: +98-09332892726
E-mail address: mosavi.a.i.buali@gmail.com (S. M. H. Mousavi)

ISSN 2816-8151 (Online) - ISSN 2816-8143 (Print)

doi: 10.5267/j.jfs.2023.1.004

airplanes as they need low operational and maintenance costs, require less space, have better access to remote areas, are fast deployable, have better maneuverability, and no need to a human pilot. All these benefits made them a proper tool for detecting and even overcoming natural disasters such as flood detection, forest fire detection, volcano activity estimation, and manmade disasters such as building fire detection and extinguishing, criminal activities applications, aerial photography, rescue applications, and more (Estrada et al., 2019). Recent UAVs are capable to carry multiple heavy colors, infrared, and thermal cameras/sensors, fire extinguishing packs, an average human, and other essential tools (SCHIEBEL CAMCOPTER, 2022). Color and thermal sensors aid UAVs to detect any heat, flame, or fire day or night and infrared sensor (Mousavi, 2018) helps to see and detect, and recognize in pure darkness plus detect the exact distance between UAV and objects which is a great advantage in dense environments like forests (Shamsoshoara et al., 2021). Also, nowadays UAVs are equipped with modern Graphical Processing Units (GPUs) which are capable to overcome complicated image processing tasks even on 4K images and videos (Hossain et al., 2019). Due to strong chips, computer vision and machine learning techniques and algorithms (Sebe et al., 2005) soared to another level and could be employed in/on small places such as UAVs. Classification (Dezfoulian se al., 2016) is of supervised learning task in Artificial Intelligence (AI) and has lots of popularity and applications among computer vision developers it means categorizing each member or sample into similar groups like differentiating between cats and dogs in an image dataset. Image segmentation (Malhotra et al., 2022) is a subset of computer vision and means to divide digital images into multiple segments or objects to achieve something meaningful and easier to analyze. In image segmentation, pixels with similar characteristics are categorized into various groups or segments and each segment indicates the specific part of the image based on texture, intensity, and color for a better understanding of human eyes and experts (Gonzalez, 2009). There are multiple image segmentation techniques from single image-based to learning based and each of them is proper for specific tasks. One of their applications is to detect fire in color or thermal sensors which could extinguish the fire ire from the background (Shamsoshoara et al., 2021). One of the main issues in fire detection in the forest is detecting small flames behind the leaves and branches from different distances and angles this paper proposed a decent method to fix these issues. Due to the lack of UAV data for wildfire, the number of research for fire detection is low but nice research has been conducted with few problems and we intended to overcome those issues. There are multiple types of research based on simple segmentation methods such as Otsu segmentation (Xiao et al., 2022), Watershed segmentation (Lin et al., 2022), K-means segmentation (Zhang et al., 2022), and deep learning segmentation (Mo et al., 2022) for wildfire detection and fire/no fire classification. Most of these researches could detect fire from UAV images just from a close distance and some don't cover fire and smoke intensity, direction, and geometrical calculation for final analysis on both color and thermal data. In this research, we are using multiple image processing techniques such as deep learning denoising (Xu et al., 2015), frequency-based features, and especially multiple nature-inspired algorithms for different stages of intensity adjustment (Gonzalez, 2009), feature extraction, segmentation, and classification to tackle these problems. The paper consisted of five main sections. Section 1 pays to the introduction (problem definition, current problems, and proposed solution). Section 2 investigates the literature and prior related research on the subject carefully. Section 3 describes the proposed method in detail. Section 4 deals with the evaluation, performance metrics, results, plots, and comparisons, and section 5 pays to the conclusion, future works, and suggestions for the final reader in order to further investigate. Table 1 presents abbreviation terms that are used in the entire paper. Based on Global Forest Watch (GFW) (GFW, 2023), tree cover loss due to all factors and fire as Mega hectare (Mha) for the years 2001 to 2021 are depicted in Fig.1. A few commonly used UAVs and sensors for forest fire detection, forest investigation, and aerial imagery are explained as follows. Specifications are as follows. A: Matrice 300 RTK, size of 810*670*430 mm, weight of 3.6 kg, speed of 51 mph, battery life of 55 minutes, operational temperature of 20°C to 40°C, infrared and color sensors with 960 p in 30 fps (Matrice, 2022). B: Phantom 4 Pro V2.0, diagonal size of 350 mm, weight of 1.3 kg, speed of 45 mph, battery life of 30 minutes, operational temperature of 0° to 40°C, infrared and color sensors with 4k resolution in 30 fps (Phantom, 2022). C: Zenmuse H20N, size of 178*135*161 mm, the weight of 875 g, supported aircraft is Matrice 300 RTK, storage of 3 SD cards up to 128 GB, operational temperature of -20° to 50° C. color sensor of 4k in 302 fps, wide sensor of full HD in 30 fps, an infrared sensor of 640*512 in 30 fps, and thermal sensor of 640*512 in 30 fps (Zenmuse, 2022). D: Parrot ANAFI Thermal, size of 242*315*64, the weight of 315 g, speed of 34 mph, battery life of 26 minutes, operational temperature of -10°C to 40°C. the color sensor of 4k and the thermal sensor of 2k (Parrot, 2022). E: INSPIRE 2, diagonal size of 605 mm, the weight of 3.4 kg, speed of 58 mph, battery life of 27 minutes, operational temperature of -20° to 40° C (INSPIRE 2, 2022). F: FLIR Vue Pro R, size of 57*44 mm, the weight of 92 g, operational temperature of -20°C to +50°C. infrared and thermal sensors of 640*512 in 30 frames (FLIR, 2022).

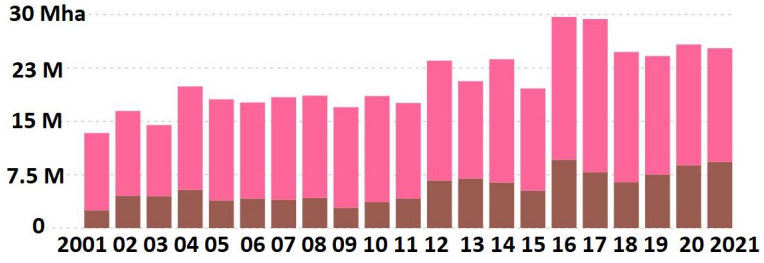


**Fig. 1.** Tree cover loss globally in Mega hectare (Mha) for years 2001 to 2021. Pink is tree loss due to all factors and brown is tree loss due to fire. Data is based on "Global Forest Watch" (GFW, 2023).

**Table 1**
Table of Abbreviations

| | |
|---|---|
| Unmanned Aerial Vehicles (UAV) | Conventional Neural Networks (CNN) |
| Graphical Processing Units (GPU) | Fire Luminosity Airborne-based Machine learning Evaluation (FLAME) |
| Millimeter (mm) | Support Vector Machines (SVM) |
| Mile per hour (mph) | K-Nearest Neighbors (K-NN) |
| Gram (g) | Chicken Swarm Optimization (CSO) |
| Kilo gram (kg) | Denoised Conventional Neural Network (DnCNN) |
| Frame per second (fps) | Bees Algorithm (BA) |
| High Definition (HD) | Local Phase Quantization (LPQ) |
| Celsius (C) | Principal Component Analysis (PCA) |
| 2-Dimensional (2-D) | Firefly Algorithm (FA) |
| Red Green Blue (RGB) | Biogeography-Based Optimization (BBO) |
| Hue Saturation Intensity (HIS) | Hue Saturation Value (HSV) |
| Extended Kalman Filtering (EKF) | Black and White (BW) |
| Unmanned Aerial System (UAS) | Suitability Index Variable (SIV) |
| Forest Fire Detection Index (FFDI) | Human Suitability Index (HIS) |
| Local Binary Patterns (LBP) | Mean Square Error (MSE) |
| Artificial Neural Network (ANN) | Positive (P), Negative (N), True Positive (TP), True Negative (TN), False |
| Histogram Equalization (HE) | Positive (FP), and False Negative (FP) |
| Probability Density Function (PDF) | Matthews Correlation Coefficient (MCC) |
| Ground Truth (GT) | Intersection over Union (IoU) |
| Structural Similarity Index Measure (SSIM) | Pearson Correlation Coefficient (PCC) |
| Gradient Conduction Mean Square Error (GCMSE) | The Peak Signal to Noise Ratio (PSNR) |
| Edge Based Image Quality Assessment (EBIQA) | Image Quality Assessment (IQA) |
| Edge and Pixel-based Image Quality Assessment metric (EPIQA) | Receiver Operating Characteristic (ROC) |
| Mega hectare (Mha) | |

## 2. Prior Related Research

The first wildfire surveillance-related research belongs to (Martínez et al., 2006). They used 3 heterogeneous UAVs: the helicopter Marvin (punctual sensor), the airship Karma, and the helicopter Heliv (visual and infrared) for Lousã (Portugal) forest fire segmentation. Their system uses simple Otsu segmentation (Xiao et al., 2022) on small data and doesn't cover fire/any fire classification, smoke detection, or fire intensity/ direction recognition. Next UAV research belongs to (Yuan et al., 2015) which pays to forest fire detection and tracking tasks. Their system uses L*a*b color space (especially "a" channel) (Mousavi et al., 2019) and some pre-processing techniques such as median filtering, morphological operations (Gonzalez et al., 2009), and Otsu segmentation. They used a small dataset and their system just segments fire on color data. (Cruz et al., 2016) modified Forest Fire Detection Index (FFDI) from detecting vegetation to detecting flame and smoke using UAV. They achieved a recognition accuracy of 96.82 % accuracy and a precision rate of 96.62 % for flame and smoke detection. (Jiao et al., 2019) made a deep learning-based forest fire detection system using Yolo V.3 (Francies et al., 2022). They Employed Conventional Neural Networks (CNN) (Bouwmans et al., 2019) Algorithm to train their model and installed it on their UAV. Also, they could successfully detect fire on their data with 83.00 % accuracy at 3.2 fps. (Yuan et al., 2019) developed a smoke detection and segmentation system based on a fuzzy (Zadeh, 1988) learning approach on Red Green Blue (RGB), and Hue Saturation Intensity (HIS) color spaces for use by UAV. Also, they used some pre-processing and post-processing techniques such as intensity adjustment, morphological operations, and Extended Kalman Filtering (EKF) to enhance their method and comparing with the Otsu method. An example of forest fire detection and classification for Unmanned Aerial System (UAS) on 4-k images belongs to (Tang et al., 2020) which employed deep learning and Yolo V.3 in order to detect small and irregular flames in high-resolution images. Their system uses two-phase learning which ends up with high computational complexity. (Hossain et al., 2020) developed a UAV-based forest fire and smoke detection system based on multi-color spaces and Local Binary Patterns (LBP) (Rahim et al., 2013) feature. They trained their system with a simple feedforward Artificial Neural Network (ANN) (Sazli, 2006) and achieved an F-score of 0.84 for flame detection and 0.90 for smoke detection. One of the greatest and most recent research in this area is belonging to (Shamsoshoara et al., 2021). They developed a firefighter assistance system called Fire Luminosity Airborne-based Machine learning Evaluation (FLAME) which offers a UAV fire dataset and techniques to segment and detect fire. They made their dataset in Arizona jungles for both color and thermal data. They used ANN for fire classification and deep learning segmentation for fire segmentation and achieved 76.23 % classification accuracy and 91.99 % precision for segmentation compared to ground truth data. Also, as their dataset is the most recent and covers color and thermal images of fire and smoke, it is subject to be used in our experiment. Another interesting and most recent UAV-based research in the area of forest fire detection and the extinguisher is conducted by (khan et al., 2022). They proposed a nice color-based fire dataset which we are using in the experiment section as the second dataset. They achieved an accuracy value of 95 %, a precision value of 95.7 %, and a recall value of 94.2 % on their data for the classification task. Also, they validate their system using different classifiers namely K-Nearest Neighbors (K-NN) (Nugrahaeni et al., 2016), random forest, naive Bayes, Support Vector Machines (SVM) (Nugrahaeni et al., 2016), and logistic regression (Bishop., 2006). (Zhang et al., 2022) proposed a system for forest fire detection and classification based on FT-ResNet50 model on transfer learning (Pan et al., 2009) and test their system on the FLAME dataset. Their deep learning method uses Adam and Mish functions (Misra, 2019) to fine-tune the convolutional blocks of ResNet (He et al., 2016) network leading to 79.48 % accuracy which is better than their comparing research. One of the most recent research projects as a firefighter assistant for a UAV subject belonging to (Ghali et al., 2022). They

made an ensemble deep learning method by combining EfficientNet-B5 (Bhawarkar et al., 2022) and DenseNet-201 (Wang et al., 2020) models in order to fire classification and segmentation tasks leading to 85 % accuracy on the FLAME dataset. Table 2 represents UAV-based related research on firefighter assistant subjects and for different tasks.

**Table 2**
Summary of Prior Related Research

| Author (s) | Fire/no-Fire Detection and Classification | Fire Segmentation (Color) | Fire Segmentation (Thermal) | Fire Intensity Recognition | Fire Direction Recognition | Smoke Detection or Segmentation | 2-D Geometrical Calculations |
|---|---|---|---|---|---|---|---|
| Martínez et al., 2006 | | ✓ | ✓ | | | | |
| Yuan et al., 2015 | | ✓ | | | | | |
| Cruz et al., 2016 | | ✓ | | | | ✓ | |
| Alexandrov et al., 2019 | | | | | | ✓ | |
| Chen et al., 2019 | ✓ | | | | | ✓ | |
| Jiao et al., 2019 | ✓ | | | | | | |
| Srinivas et al., 2019 | ✓ | | | | | | |
| Yuan et al., 2019 | | | | | | ✓ | |
| Barmpoutis et al., 2020 | | ✓ | | | | ✓ | |
| Hossain et al., 2020 | ✓ | | | | | ✓ | |
| Tang et al., 2020 | ✓ | ✓ | | | | | |
| Frizzi et al., 2021 | | ✓ | | | | ✓ | |
| Shamsoshoara et al., 2021 | ✓ | ✓ | ✓ | | | | |
| Ghali et al., 2022 | ✓ | ✓ | | | | | |
| Khan et al., 2022 | ✓ | | | | | | |
| Zhang et al., 2022 | ✓ | | | | | | |
| Proposed | ✓ | ✓ | ✓ | ✓ | ✓ | ✓ | ✓ |

## 3. Proposed Method

The proposed method consists of three main parts of fire segmentation, fire/no fire classification, and smoke detection. Each part includes multiple stages of image processing techniques and algorithms. Also, fire intensity and direction recognition plus 2-D geometrical properties of segmented fire are a subset of the fire segmentation part. The main motivation of this experiment is to forest monitoring and control for surveillance and safety application which could be applied to software aspects in UAVs. In that way, forest fire or wildfire could be detected in the early stages, and by extinguishing it more lives (firefighters, civilians, and animals) and natural environments could be saved.

### *3.1 Fire Segmentation*

The proposed forest fire segmentation method starts with Chicken Swarm Optimization (CSO) Algorithm (Meng et al., 2014) and Intensity Adjustment (Vamsidhar et al., 2022) in order to enhance the image and reveal all elements and components for further investigation and analysis. CSO intensity adjustment shows better performance compared with traditional and even other nature-inspired techniques for this topic. Also, CSO contrast enhancement is proper for images in dense environments like forests. CSO algorithm consists of three main elements (a dominant rooster, multiple hens, and multiple chicks). Hens and chickens are randomly distributed in groups for the first generation but sorted and select in the next generations. Chickens follow their group rooster for food and sometimes steal each other food. Chicks, however, follow their mother for finding food. Dominant roosters fight over the best group and food.

In order to increase elements separability in the digital image, a sharpening technique called unsharp masking (Polesel et al., 2000) applies to an image which helps to separate fire better from the background. Unsharp masking has roots in dark-room or analog photography but now has applications in image processing due to its decent performance. The base of unsharp masking comes from subtracting a lowpass or blurred image from the original image in order to create a mask which uses to sharpen the image. There are two main parameters of radius and amount for unsharp masking which here a radius of 1.5 and an amount of 1.2 is used by the algorithm. Radius is the Standard Deviation (SD) around an average of the gaussian value for the low pass which considers pixel edges and the amount determines the power of the affected filter. Considering the edge image of g(x,y) for the image of f(x,y) and k as scaling constant then, the unsharpened image would be as Eq. (1).

$$unsharp\ masked\ image(x,y) = f(x,y) + k * g(x,y) \tag{1}$$

Sharpening is followed by the Denoising Conventional Neural Network (DnCNN) (Zhang et al., 2017) algorithm for getting rid of any unwanted pixels for the main process. DnCNN is a pretrained model basically for gaussian noises but it performs well on other types of noise, too. The employed DnCNN structure with 59 layers is represented in Fig. 2.

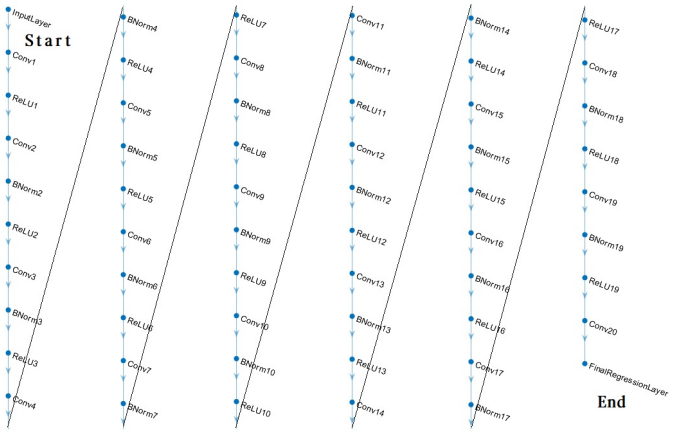


**Fig. 2.** Employed DnCNN Structure for denoising task with 59 layers

Nature-inspired algorithms (Zang et al., 2010; Mousavi and Mirinezhad, 2022) normally are mathematical models of animals/insects' social behavior or they could be evolutionary-based, human-based, and even Physical laws-based in a manner that leads problems to an optimal solution during iterations by a specific number of populations in each generation. These algorithms could be employed in multiple optimizations (Mousavi et al., 2017) tasks, such as regression, clustering (Mousavi et al., 2017)[2], feature selection, Minimum Spanning Tree (MST) (Mitchell et al., 1997), Hub Location Allocation (HLA) (Sadeghi et al., 2018), and more. One of these Nature-inspired algorithms which have high efficiency is called Bees Algorithm (BA) (Pham et al., 2006). BA has a lot of applications and BA, simply implements the social behavior of honey bees to search (in a neighborhood manner) for food in flowers. Agents, Scouts, and Forager bees are involved in global and local searches to reach the best solution. The waggle dance is done by scouts which found the best sites. Those who landed on elite sites, recruit new members. The list of best bees based on local and global goes to the next generation and the cycle stops by termination criterion's conditions.

The segmentation part is conducted by Bees Algorithm (BA) image segmentation (Dragaj, 2016) as it performs more robustly and faster than other algorithms. As BA consists of local and global searches, first it finds segments in the global search and then improved in the local search which makes it unique compared to other algorithms. Fig. 3 depicts flowcharts of CSO contrast enhancement and Bees image segmentation.

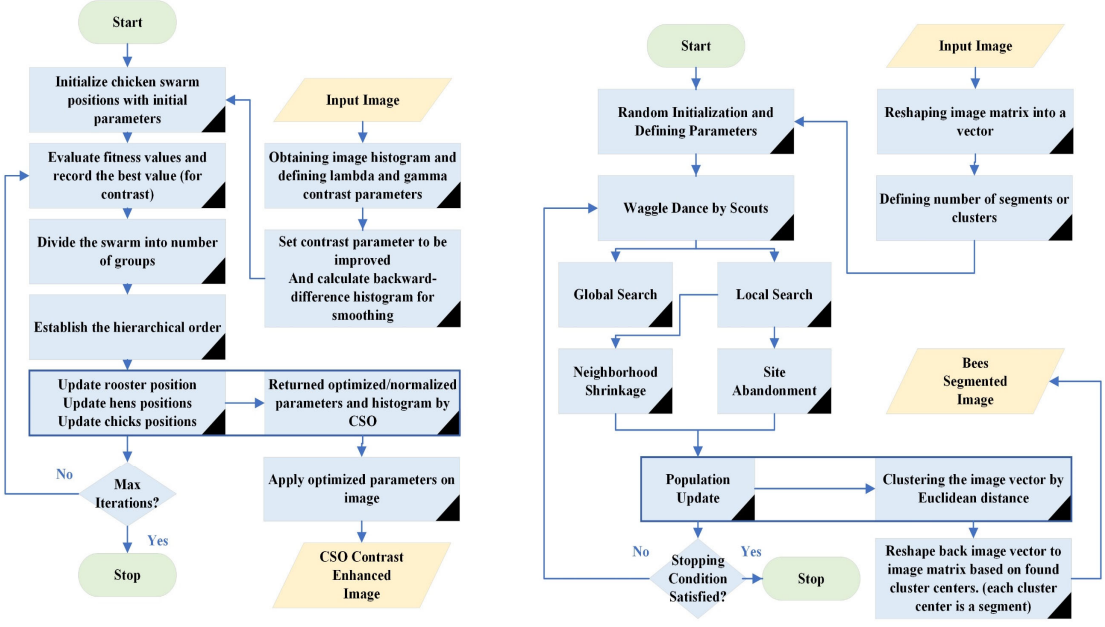


**Fig. 3.** CSO contrast enhancement flowchart on the left and Bees image segmentation flowchart on the right

Alongside fire segmentation, fire intensity and fire direction recognition are considered which aids to follow the fire's path and its destination. Fire intensity is the area or the real number of pixels in the region from the center of the fire (in Black and White (BW) image) and fire direction is the angle between the x-axis and the major axis of an ellipse that has the same

second-moments as the region in degree. Also, some 2-D geometrical calculations namely, major axis length, minor axis length, equal diameter, perimeter, solidity, and extent for flames will be calculated which helps firefighters to analyze fire even better.

Considering segmented fire as a 2-D BW region, the orientation would be an ellipse that fits inside the fire region with a degree of its bigger radius. Now major axis length is the bigger radius length in pixels and the minor axis length is the smaller radius in pixels. Now, considering the area of the region by the number of pixels in the region, then equal diameter would be the diameter of a circle with the same area as the region (4/area*pi). Perimeter is the distance around the boundary of the region and solidity is the proportion of the pixels in the convex hull (Gonzalez et al., 2009) that are also in the region. Finally, the extent is the ratio of pixels in the region to pixels in the total bounding box. Fig. 4, depicts a sample from the FLAME dataset which is segmented by the proposed method. Also, fire intensity and direction are calculated and overlayed on the segmented image. Fire intensity is represented by the red circle and fire intensity by the dashed blue line. 2-D geometrical calculations for this experiment are as follow: Area is: 12693, Orientation is: 30.2548, Major Axis Length is: 277.0042, Minor Axis Length is: 74.3609, Equal Diameter is: 127.1268, Perimeter is: 759.088, Solidity is: 0.61959, and Extent is: 0.2856. Fig. 5 illustrated the proposed forest fire segmentation method as a flowchart. Also, Fig. 6 represents the proposed segmentation steps on a color sample image from the FLAME dataset. Also, Fig. 7 represents the proposed method on two green and white thermal samples from the FLAME dataset. Table 2 shows CSO image contrast adjustment and Bees image segmentation pseudo codes.

$$Fire\ Intensity = Area = \sum pixels\ (BW(x, y)) \tag{2}$$

$$Fire\ Direction = Max\ (ellipse\ axis)\ degree\ from\ fire\ center \tag{3}$$


**Fig. 4.** An experiment result by proposed fire segmentation. a): Original image, b): boundary over segmented part, c): Fire segmentation, intensity, and direction recognition by proposed method (intensity is 12693 pixels and direction are 30 degrees).

**Table 2**
CSO image contrast adjustment and Bees image segmentation pseudo codes

| CSO Intensity Adjustment Pseudo Code | Bees Image Segmentation Pseudo Code |
|---|---|
| *Start*<br>*Load input image*<br>*Obtain image histogram*<br>*Calculate backward difference histogram*<br>*Generating initial population*<br>*Define CP (Contrast Parameters of lambda and gamma)*<br>*While max iteration is not satisfied*<br>*Evaluating the population based on fitness function (normalized*<br>*Divide the swarm into a number of groups*<br>*Establish the hierarchical order*<br>*Update rooster position*<br>*Update hens' position*<br>*Update chicks' position*<br>*Sorting (Best CPs)*<br>*End While*<br>*Select the most optimized CP*<br>*Apply the selected CP on image*<br>*End* | *Start*<br>*Load input image*<br>*Reshape the image into vector*<br>*Generating initial population*<br>*Define NS (number of segments or clusters)*<br>*Evaluating the population based on fitness function (cluster distances)*<br>*Sorting*<br>*While max iteration is not satisfied*<br>*Select elite patches and non-elite best patches for local search*<br>*Recruit forager bees for elite patches and non-elite best patches*<br>*Evaluate the fitness value of each patch*<br>*Sorting (Best cluster centers)*<br>*Allocate the rest of the bees for global search*<br>*Evaluate the fitness value of non-best patches*<br>*Sorting (Improving cluster centers)*<br>*End While*<br>*Select best cluster centers (equal to NS)*<br>*Reshaping image vector to image matrix*<br>*Allocating found cluster centers to each pixel*<br>*End* |

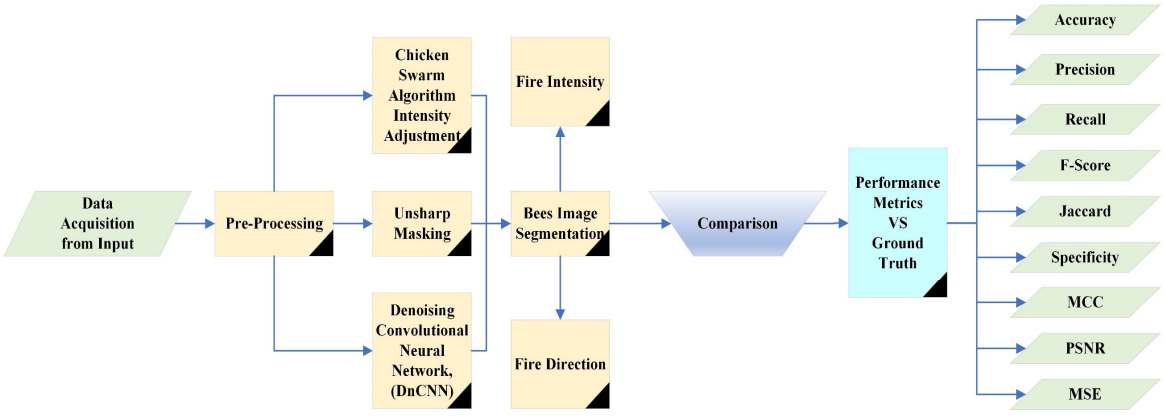


**Fig. 5.** Flowchart of the proposed forest fire segmentation method

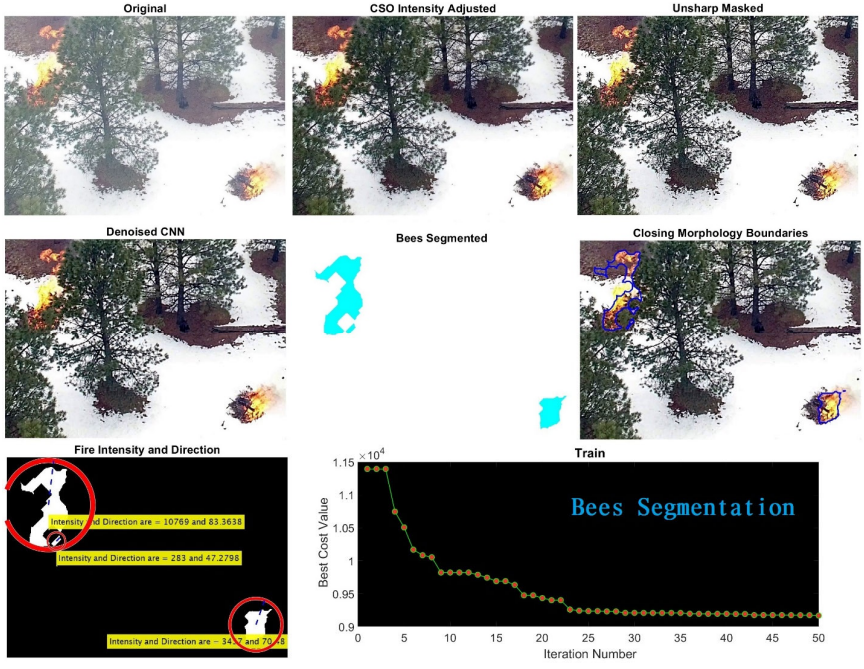


**Fig. 6.** Proposed segmentation steps on a color sample from the FLAME dataset (4 segments, population of 5, 50 iterations, and mutation rate of 0.2).

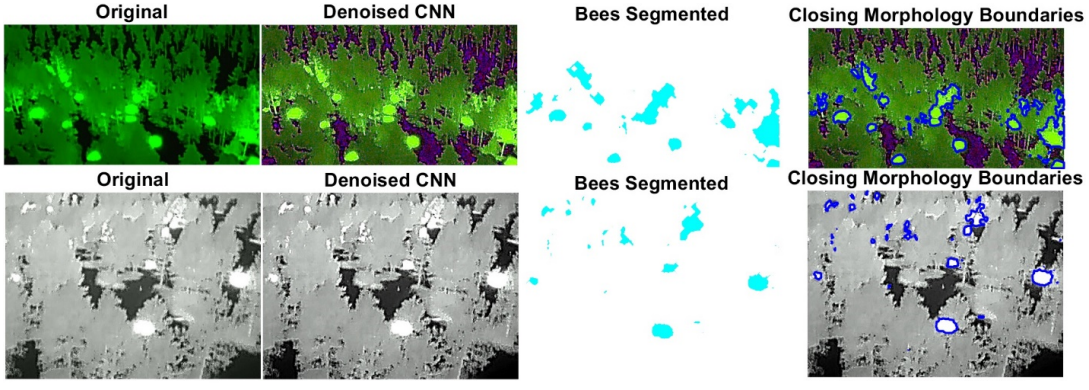


**Fig. 7.** Proposed segmentation steps on two thermal samples from the FLAME dataset (3 segments, population of 5, 50 iterations, and mutation rate of 0.2).

### *3.2 Fire Classification*

For the fire/ no fire classification part, training data pass through gray level conversion for faster processing followed by resizing and DnCNN denoising technique to get rid of any unwanted pixels. Denoised images pass through some similarity performance techniques in order to check if data is clean enough plus evaluate the performance of the denoising step. As just two classes of fire and no fire exists, using computationally complex methods such as deep neural network techniques are unnecessary and here shallow neural networks would be enough. In order to extract more robust features, frequency domain (Bergland, 1969) features are used and Local Phase Quantization (LPQ) features (Yuan et al., 2012) satisfy the problem, here. LPQ is a frequency neighborhood-based feature based on Fourier transform (Bracewell et al., 1986). It manipulated the blurring effect in magnitude and phase channels. Phase channel is capable of deactivating low pass filters that exist in some images. LPQ features are perfect to be used on color, thermal, and depth or infrared data in the frequency domain. LPQ extracts 256 features which is more than enough for two classes, that's why the number of features should be reduced to half or a quarter by dimensionally reduction or feature selection techniques (Chandrashekar et al., 2014). Fig. 8 presents the workflow of LPQ feature on a sample image.

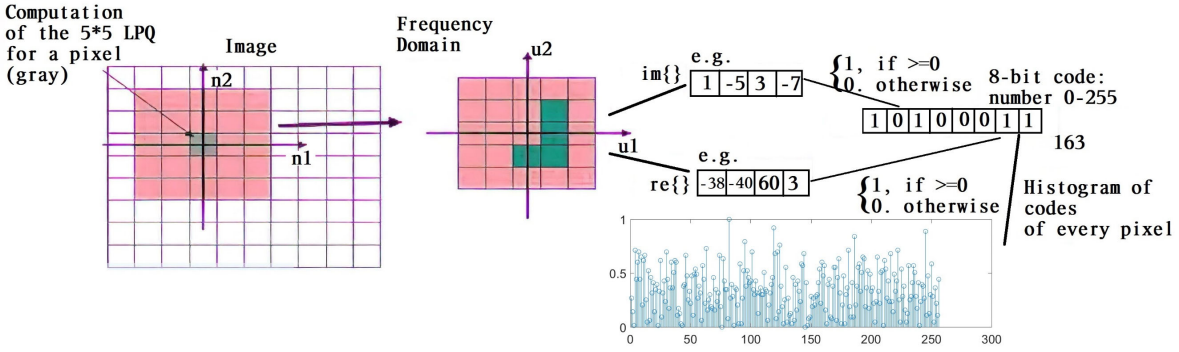


**Fig. 8.** LPQ algorithm workflow

It has to be mentioned feature selection techniques clean data from outliers (Chandrashekar et al., 2014). There are lots of feature selection methods such as Principal Component Analysis (PCA) (Abdi & Williams, 2010), Lasso Regularization (Tibshirani, 1996), Fisher (Sun et al., 2021), and more but in order to select the most impactful features, a more robust approach which is a learning-based approach is needed. Nature-inspired feature selection techniques are among the best in learning-based feature selection techniques. Based on our experiments, Biogeography-Based Optimization (BBO) (Simon, 2008) is the best among others for feature selection tasks that are employed in our experimental research (Rostami et al., 2021). The BBO algorithm consists of important parameters of the number of Habitants or "H", Human Suitability Index or "HIS", Emigrations Rate or μ, Immigration rate or λ, and Suitability Index Variable (SIV). This algorithm is all about moving living creatures from one habitat to another with better living conditions and room to grow. In feature selection, we are dealing with the Number of Features of "NF", the weight of the feature or "w" and Mean Square Error (MSE) (Skowronski et al., 2006) which should be minimized to select the feature. Also, if $x_i$ is the value of NF then, $\hat{x_i}$ would be selected features out of NF. So, considering the number of features entering the system, "y' would be the output, and "t" would be the target. In order to calculate the final error, $e_i$ needs to be calculated which is $t_i$ - $y_i$ . So final error is $\min MSE = \frac{1}{n}\sum_{i=1}^{n} e_i^2$+w*NF. This goes for all features and finally, those features with the lowest MSE will be selected. In combination with BBO and feature selection, each feature vector is considered a habitant with a different HIS. Those habitats which could fit into the final iteration would be selected alongside their related features with lowers error as mentioned.

After feature selection, there would be binary classification (Dezfoulian et al., 2016) for fire / no fire data which leads to a labeling task for classification. Data is divided into 70 % / 30% for training and testing stages. Also, Artificial Neural Network (ANN) (Mitchell et al., 1997) structure is based on just 12 neurons with resilient backpropagation (Almiani et al., 2022) structure. After learning by ANN, it is possible to improve the weights and biases of the model by nature-inspired algorithms. Here, Firefly Algorithm (FA) (Yang, 2010) algorithm is employed for this improvement after the learning process as it is faster and more precise than most of the other algorithms. FA consists of five main parts of the number of population (fireflies) or x, the light intensity of each firefly or I, light absorption coefficient or γ, attraction coefficient or β, and mutation rate. It simply works as moving lower light-intensity fireflies toward higher ones, affecting mutation and updating old and new solutions. Fig. 9 represents the BBO feature section and FA classification flowcharts. Fig. 11 presents the structure of an ANN. Also, Fig. 10 depicts the whole process of the proposed classification workflow. Table 3 shows BBO feature selection and FA classification as pseudo-code.

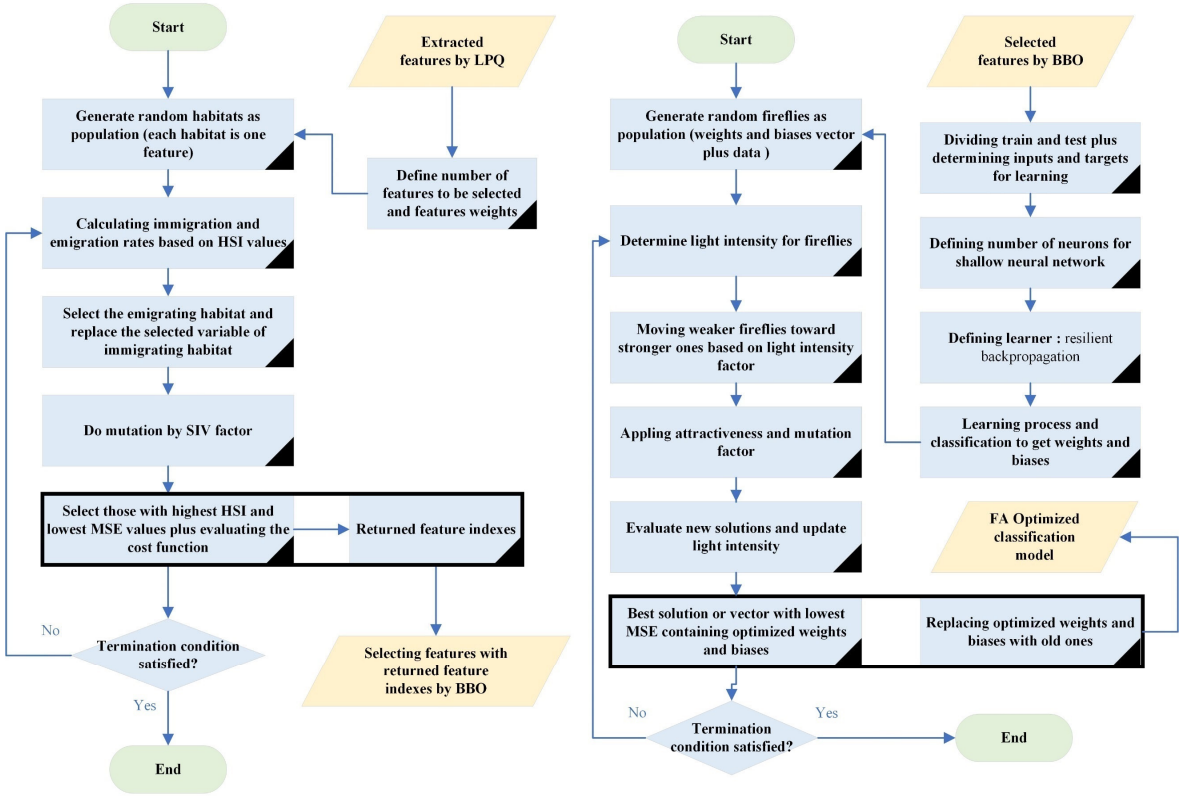


**Fig. 9.** BBO feature selection flowchart in the left and the FA classification flowchart in the right

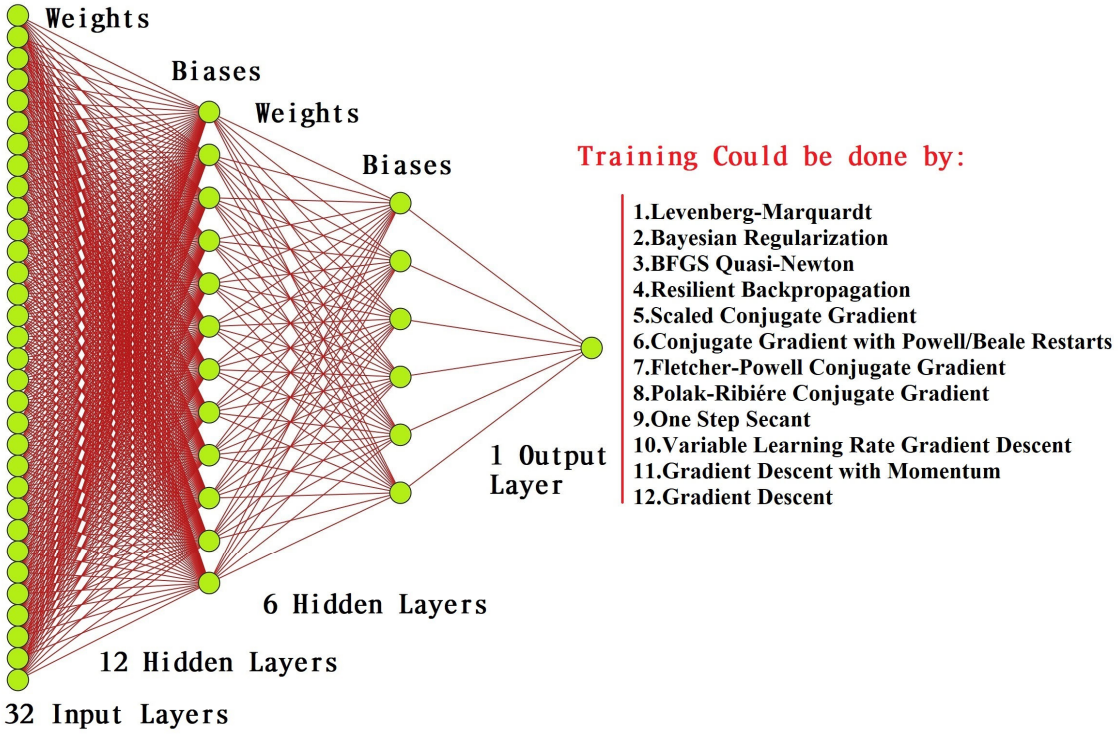


**Fig. 10.** The structure of common ANN

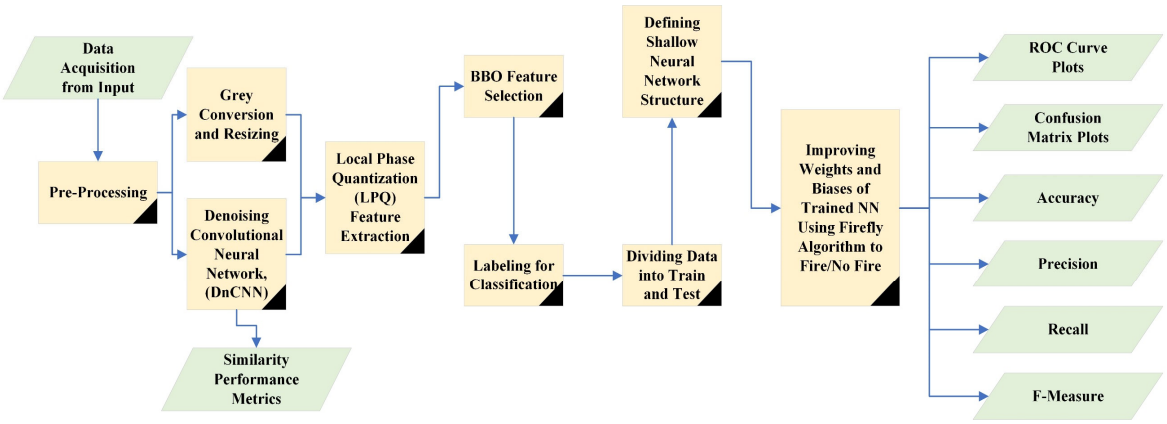


**Fig. 11.** Proposed fire/ no fire classification workflow

**Table 3**
BBO feature selection and FA classification as pseudo codes

| BBO Feature Selection Pseudo Code | FA Classification Pseudo Code |
|---|---|
| *Start*<br>*Load data (LPQ Feature)*<br>*Generate a random set of habitats (H1, H2, …, Hn (Features)*<br>*Define FN (number of features) and w (weights for Feature)*<br>*Compute HSI value (Fitness function and sort best to worst)*<br>*While termination criterion is not satisfied*<br>*Keep the best individuals (elites (best Features))*<br>*Calculate immigration rate λ and emigration rate μ for each habitat based on HSI*<br>*Start Migration*<br>*Select Hi with probability by λ*<br>*Select Hj with probability by μ*<br>*Randomly select a SIV from Hj*<br>*Replace random SIV Hj with Hi*<br>*End of migration*<br>*Start Mutation*<br>*Select a SIV in Hi with probability of mutation rate*<br>*If Hi (SIV) is selected*<br>*Replace Hi (SIV) with a randomly generated SIV*<br>*End if*<br>*End of Mutation*<br>*Recalculate the HSI value of new habitats*<br>*Calculate MSE of Features*<br>*Sort population (best to worst (cost))*<br>*Replace worst with preview generation's elites (Features with best cost)*<br>*Sort population (best to worst (cost))*<br>*End of while*<br>*Select NF first ones*<br>*End* | *Start*<br>*Load Data (BBO Selected Features)*<br>*Diving Train and Test data (Both into Inputs and Targets)*<br>*Define number of neurons and learn using resilient backpropagation algorithm to get basic weights and biases*<br>*Goal: Improving weights and biases*<br>*Objective function f (x), x=(x1,x2,…,xd)$^T$*<br>*Generating population of fireflies xi (i=1,2,…,n) (weights and biases vector)*<br>*Define light intensity Ii in xi by f(xi)*<br>*Define light absorption coefficient γ or gamma*<br>*While maximum generation is not satisfied*<br>*For i=1 to n fireflies*<br>*For j=1 to n fireflies (inner loop)*<br>*If (Ii < Ij), firefly i goes toward firefly j*<br>*End if*<br>*Change attractiveness by distance of r via exp [- γr]*<br>*Evaluate new solutions and update light intensity*<br>*End*<br>*End*<br>*Sort and rank fireflies and find the current global best or g**<br>*End of while*<br>*Getting Optimized Value of $p_i^* = x_i p_i^o$*<br>*($x_i$ by Firefly Algorithm and $p_i^o$ by Fuzzy Logic)*<br>*Returning optimized solution vector with lowest MSE containing optimized weights and biases*<br>*Replacing optimized weights and biases with basic ones*<br>*Classification using FA optimized model*<br>*End* |

### *3.3 Smoke Detection*

A color space explains the span of colors, that a camera sensor can observe, a printer machine can publish, or a screen can present (Mousavi et al., 2019). The proposed smoke detection procedure starts with separating channels of Red, Green, and Blue (RGB) color space and improves the contrast of each channel with the Histogram Equalization (HE) (Dhal et al., 2021) technique followed by median filtering (Mousavi et al., 2017) as it helps to reveal smoke mass better. It has to be mentioned that RGB color space is widely used because of its ease of use, wide application, and easy comprehension for wide range of audience. Histogram equalization is a contrast enhancement technique that tries to distribute image histogram bins evenly which lets for areas with low local contrast to achieve a higher local contrast. Also, median filtering is a low-pass filter that removes noises by keeping most of the edges in the image. In contrast to DnCNN which was proper for removing Gaussian noises, median filtering is proper for removing salt and pepper noise. Considering $f_{i,j}$ as original image, $n$ as the number of pixels, $L$ as the number of intensity values, and $p$ denotes the normalized histogram of $g$ with a bin for every intensity values. Then HE would be as Eq. (4):

$$HE = g_{i,j} = \text{floor}\left((L-1)\sum_{n=0}^{f_{i,j}} p_n\right) \tag{4}$$

Gaussian noise (Mousavi et al., 2019) is a type of noise containing a Probability Density Function (PDF) same as the normal distribution value, that is known as the Gaussian distribution. The PDF of a Gaussian random variable Z is as below Eq. (5):

$$Gaussian\ noise = P_g(Z) = \frac{1}{\sigma\sqrt{2\pi}} e^{\frac{(Z-\mu)^2}{2\sigma^2}} \tag{5}$$

In which Z is the grey level, $\mu$ is the mean, and $\sigma$ represents the SD value. Now, Salt-and-pepper noise (Mousavi et al., 2019) which is also known as impulse noise is another common image noise. This kind of noise will be caused by sharp and sudden disorder in the image receiving signal. It appears as scattered black and white pixels. It could be eliminated by median filtering technique.

$$Salt - and - pepper\ noise = P(Z) = \begin{cases} P_a & for\ \ z = a \\ P_b & for\ \ z = b \\ 0 & otherwise \end{cases} \tag{6}$$

Having “b” value higher than “a” value, then gray level “b” appears as a very light dot on image. If either $P_a$ or $P_b$ having value of zero, then this is called unipolar type of noise. If none of $P_a$ or $P_b$ is zero and if they have almost equal values, then the noise is called salt & pepper. Fig. 12 illustrates the performance of median filtering and DnCNN denoising technique on a sample polluted with gaussian and impulse noises.

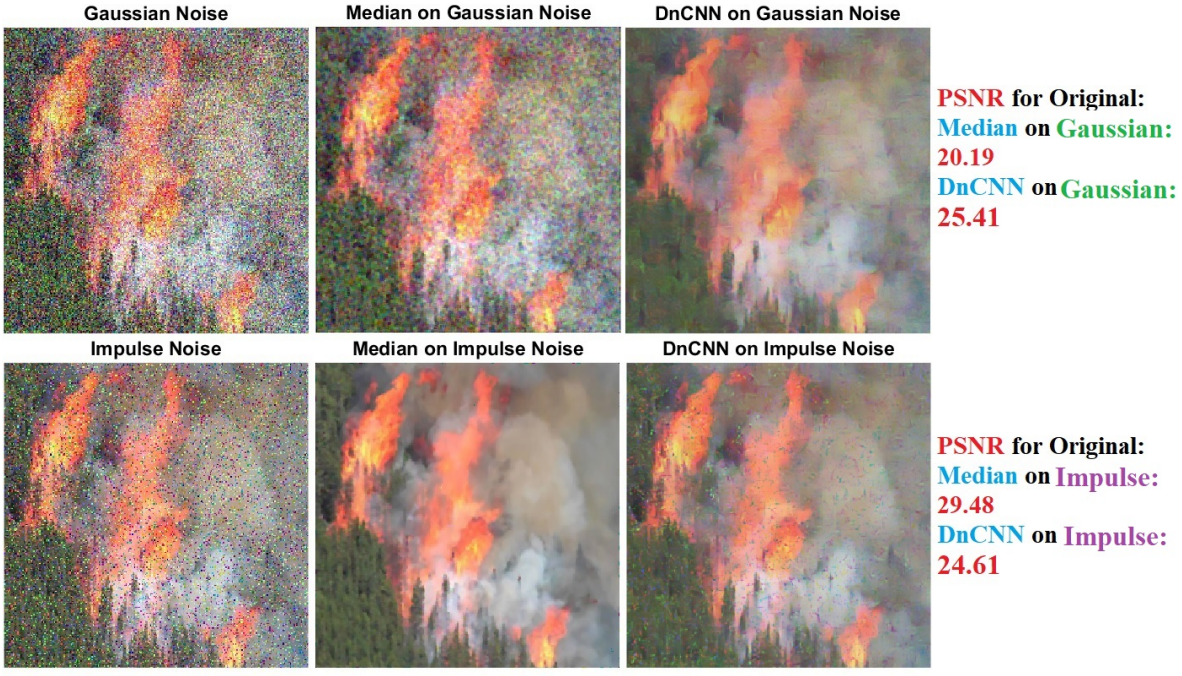


**Fig. 12.** Performance of median filter and DnCNN denoising on polluted image with gaussian (mean of 0 and variance of 0.05) and impulse (noise density of 0.1) noises.

After pre-processing, all three channels combine together and convert into three color spaces of Hue, Saturation, Value (HSV), Lab, and YCbCr (Busin et al., 2008). HSV color space is a replacement for RGB and was made in the 1970s which mimics human vision color understanding and Hue or H channels could distinguish smoke mass in an image. Having YCbCr color space, Y value is the luma element, and Cb-Cr are the blue-change and red-change chroma element that Cb is a smoke distinguisher channel. Now, each color space separates into three channels which makes a total of nine channels. Now, the CIELAB space of color (which is known as CIE L*a*b* or in summery "Lab" color space) is a color space introduced by the International Commission on Illumination (CIE) in 1976 (Tkalcic et al., 2003). It illustrates colors as three numerical values of L* for the lightness and a* and b* for the green–red and blue–yellow color elements which we need just the “a” component. Three channels of Hue, Cb, and an of these nine channels which are the most effective channels for smoke emergence will be selected to create one color image. Finally, by applying opening morphology (Gonzalez, 2009), the final smoke mass reveals. Fig. 13 represents the proposed smoke detection workflow. Fig. 14 and Fig. 15 illustrate the HE results on two color and thermal sample images alongside their related image histogram before and after the HE processes plus their corresponding transformation curve. Fig. 16 depicts a sample image from Deep Fire dataset in RGB, HSV, YCbCr, and Lab color spaces as a whole and separated channel. Also, Fig. 17 represents the proposed smoke detection workflow on a sample image from Deep Fire dataset.

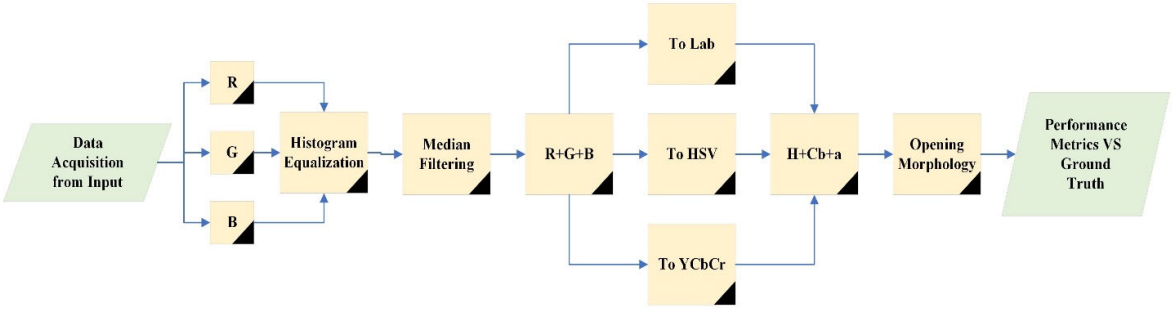


**Fig. 13.** Proposed smoke detection workflow

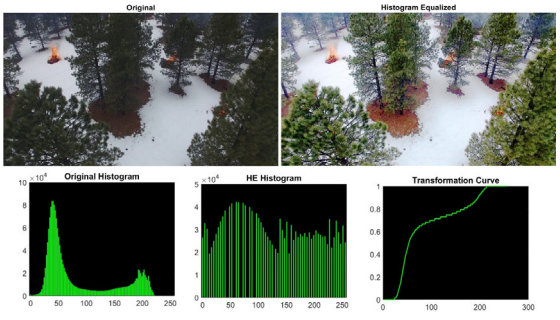


**Fig. 14.** Original and result after applying HE on a color sample image from FLAME dataset alongside with image histograms and corresponding transformation curve

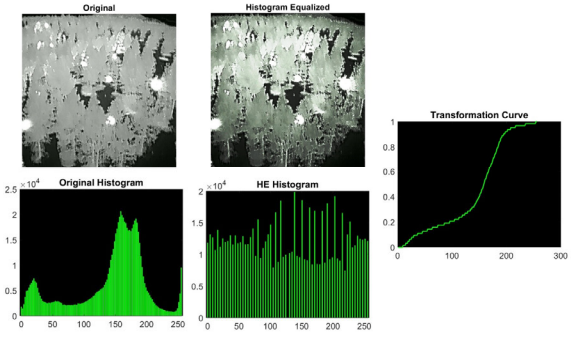


**Fig. 15.** Original and result after applying HE on a thermal sample image from FLAME dataset alongside with image histograms and corresponding transformation curve

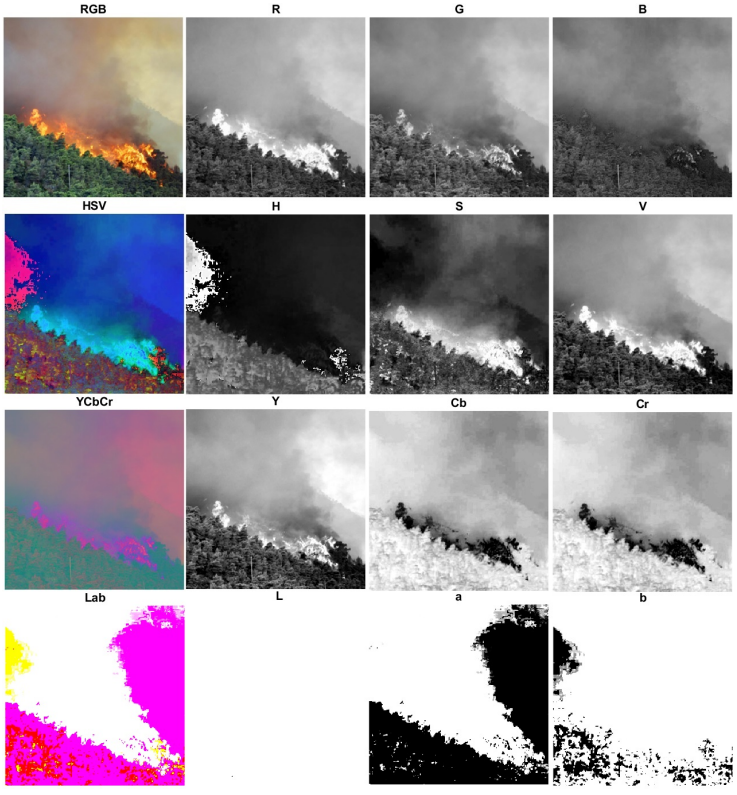


**Fig. 16.** Sample image from Deep Fire dataset in RGB, HSV, YCbCr, and Lab color spaces as whole and separated channels

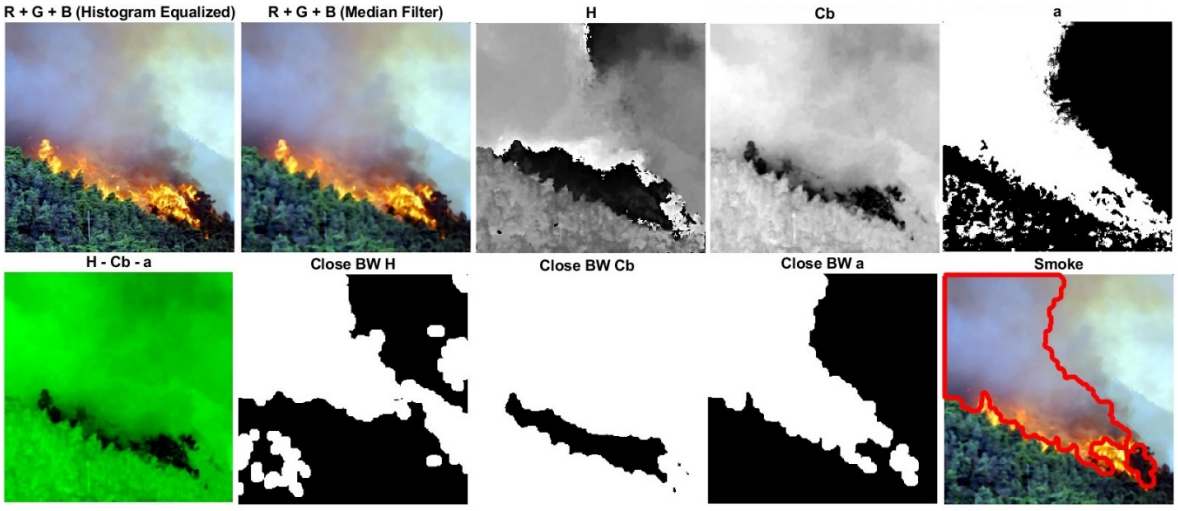


**Fig. 17.** Proposed smoke detection workflow on a sample image from Deep Fire dataset

## 3. Evaluations and Results

For all three approaches of fire segmentation, fire classification, and smoke detection, the two most recent UAV-based fire datasets of FLAME by Shamsoshoara et al. (2021) and DeepFire by (Khan et al., 2022) are employed for evaluation validation of the proposed methods. Dataset's main characteristics are mentioned in Table 4. It has to be mentioned that fire segmentation and classification for thermal data of the FLAME dataset have been done for the first time in this research. Also, the smoke detection approach for both datasets is been done for the first time in this research. Additionally, the amount of data used in the experiment is explained in Table 5.

**Table 4**
Datasets Characteristics

| Dataset | Color data | Thermal data | Task(s) |
|---|---|---|---|
| **FLAME**<br>**Shamsoshoara et al., 2021** | 39,375 images with resolution of 254*254 for train and 8617 images for test – 2003 images for segmentation and 2003 mask images as ground truth. | Thermal white in 89 seconds and thermal green in 305 seconds both in 640*512 resolution. | Fire Segmentation<br>Fire Classification<br>Smoke Detection |
| **DeepFire**<br>**Khan et al., 2022** | 1900 images – Resolution of 250*250 | None | Fire Segmentation<br>Fire Classification<br>Smoke Detection |

**Table 5**
Data used in the experiment

| Dataset | Color data | Thermal data |
|---|---|---|
| **FLAME**<br>**Shamsoshoara et al., 2021** | 39,375 color images for fire classification as train and 8617 color images as test, 2003 color images for fire segmentation, and 500 color images for smoke detection. | 200 thermal white and 300 thermal greens for fire segmentation and classification |
| **DeepFire**<br>**Khan et al., 2022** | 1900 color images for fire classification (1520 images for train and 380 images for test), 500 color images for fire segmentation, and 500 color images for smoke detection. | None |

In order to validate the proposed segmentation method's final result, the predicted output should be transformed into a BW image for compare with the mask or Ground Truth (GT) BW image. Also, there are definitions such as Positive (P), Negative (N), True Positive (TP), True Negative (TN), False Positive (FP), and False Negative (FP) (Wang et al., 2020) which are needed for evaluation. P is the real number of positive cases and N is the real number of negative cases in the image. By considering white color or 1 as positive and black color or 0 as negative in the BW image, TP is when the model correctly predicts the positive class and TN define when model correctly predicts the negative category. Now, the FP belongs to a situation in which the model incorrectly predicts the positive category and FN is when the model incorrectly predicts the negative category (Powers., 2020). Fig. 18 shows mentioned concept as visual.

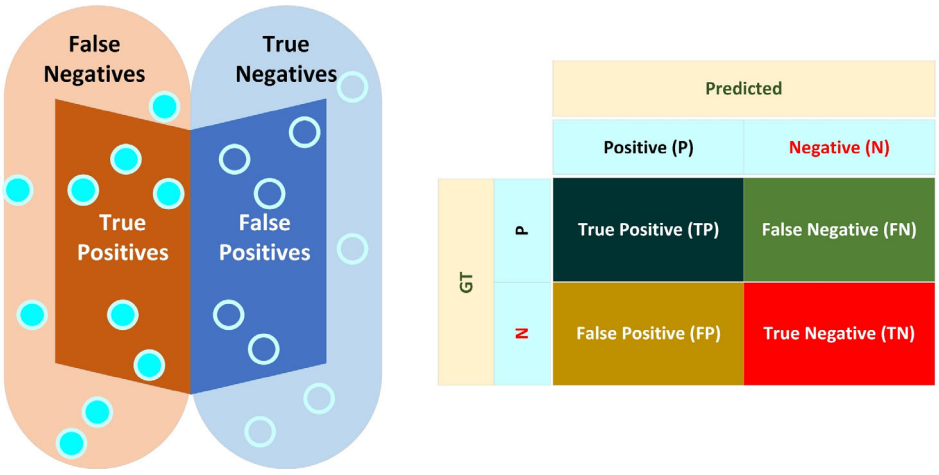


**Fig. 18.** Ground Truth, Predicted, TP, FN, FP, and TN as a visual

Now, accuracy is the percent of pixels that are correctly classified as EQ. (7):

$$Accuracy = \frac{TP + TN}{TP + TN + FP + FN} \tag{7}$$

Precision means how many of those predicted objects had matching ground truth annotation and is calculated as Eq. (8):

$$Precision = \frac{TP}{TP + FP} \tag{8}$$

Recall or sensitivity means of all objected annotated in the ground truth, how many are captured as positive predicator and is calculated a Eq. (9):

$$Recall = \frac{TP}{TP+FN} \tag{9}$$

The F1 score or BF measure illustrates how properly the predicted boundary of all categories aligns with the real boundary. The F1 score is specified as the precision plus recall values with a distance error endurance and shows as Eq. (10):

$$F1 - Measure = \frac{2*TP}{2*TP+FP+FN} \tag{10}$$

Now, Intersection over Union (IoU) (Setiawan., 2020) metric, or the Jaccard similarity coefficient, undoubtedly is one of the most universally used metric for segmentation purpose. IoU metric is an actuarial correctness measurement that is against the false positives. For all categories or classes, IoU is the ratio of rightly categorized pixels to the all number of GT and predicted pixels in that specific category based on Eq. (11):

$$IoU = \frac{F1 - Measure}{2 - F1 - Measure} \tag{11}$$

Just like sensitivity, specificity another great metric in order classify corrected parts ad is calculated as Eq. (12):

$$Specificity = \frac{TP}{TN+FP} \tag{12}$$

Matthews Correlation Coefficient (MCC) (Matthews., 1975) is a measure of association for two binary images. Pearson Correlation Coefficient (PCC) (Benesty et al., 2009) estimated for two binary variables will return MCC as Eq. (13):

$$MCC = \frac{TP*TN-FP*FN}{\sqrt{((TP+FP)*(TP+FN)*(TN+FP)*(TN+FN))}} \tag{13}$$

The Peak Signal to Noise Ratio (PSNR) (Joshi et al., 2016) indicates the level of data loss or signals totality. This measure is in decibels and for two images. This ratio value is often used as a modality measurement for the original and a compressed image but it can be used for two BW images as Eq. (14):

$$PSNR = 10log_{10}\frac{L^2}{MSE} \tag{14}$$

In Eq. (14), L defines the range of possible pixel value in an image, and has a limit of 50. A good value could be in range of 20 and 50. The higher value, the better. The Mean Square Error (MSE) factor depicts the cumulative squared error for the two compressed and the original image (here predicated and ground truth images). Having lower the value of MSE, means more proper evaluation and it calculates as Eq. (15).

$$MSE = \frac{1}{M \times N} \sum_{i=0}^{N-1} \sum_{j=0}^{M-1} [X(i,j) - Y(i,j)]^2 \tag{15}$$

In which, *X* and *Y* are two arrays with the size of M*N (images). To any extent Y resembles X, the value of MSE will reduce. Tables 6 and 7 show acquired evaluation results by the proposed segmentation method alongside with comparison with traditional and famous segmentation techniques for color and thermal data of the FLAME dataset. The same for the DeepFire dataset is presented in Table 9. Fig.19 depicts some acquired results of fire segmentation and smoke detection in comparison with ground truth data. It has to be mentioned that ground truth data for thermal and smoke images are done manually as there were no such masks or data available. Table 9 represents parameters that are used by different nature-inspired algorithms for different tasks in the experiment. Returned results by the proposed segmentation method on all data in all Tables show superiority over other methods. Fig. 20 represents CSO contrast enhancement and Bess image segmentation techniques' performance in 100 iterations on two color and thermal test samples from the FLAME dataset.

**Table 6**
Fire segmentation results on color data of FLAME dataset with comparisons

| | Accuracy | Precision | Recall | F1-Measure | IoU | Specificity | MCC | PSNR | MSE |
|---|---|---|---|---|---|---|---|---|---|
| **Otsu** | 94.70 | 85.16 | 78.91 | 83.64 | 72.41 | 91.58 | 93.61 | 27.14 | 0.057 |
| **K-Means** | 92.36 | 83.90 | 76.55 | 81.11 | 71.37 | 89.71 | 91.20 | 23.99 | 0.119 |
| **Shamsoshoara et al., 2021** | - | 91.99 | 83.88 | 87.75 | 78.17 | 99.96 | - | - | - |
| **Proposed** | 99.95 | 95.57 | 97.89 | 97.73 | 95.57 | 99.97 | 97.74 | 40.31 | 0.002 |

**Table 7**
Fire segmentation results on Thermal data of FLAME dataset with comparisons

| | Accuracy | Precision | Recall | F1-Measure | IoU | Specificity | MCC | PSNR | MSE |
|---|---|---|---|---|---|---|---|---|---|
| **Otsu** | 95.62 | 74.25 | 88.14 | 80.36 | 70.48 | 95.55 | 81.97 | 26.11 | 0.052 |
| **K-Means** | 93.74 | 72.22 | 86.78 | 79.37 | 69.20 | 92.39 | 78.66 | 21.40 | 0.099 |
| **Shamsoshoara et al., 2021** | - | - | - | - | - | - | - | - | - |
| **Proposed** | 99.01 | 78.59 | 91.59 | 84.59 | 73.30 | 99.23 | 84.35 | 31.60 | 0.008 |

**Table 8**
Fire segmentation results on DeepFire dataset with comparisons

| | Accuracy | Precision | Recall | F1-Measure | IoU | Specificity | MCC | PSNR | MSE |
|---|---|---|---|---|---|---|---|---|---|
| **Otsu** | 93.88 | 91.74 | 93.57 | 92.71 | 89.16 | 91.72 | 92.60 | 27.77 | 0.066 |
| **K-Means** | 94.14 | 92.00 | 93.97 | 93.01 | 91.19 | 91.99 | 93.67 | 29.02 | 0.034 |
| **Proposed** | 98.16 | 96.77 | 99.84 | 98.28 | 96.62 | 96.28 | 96.36 | 33.90 | 0.017 |

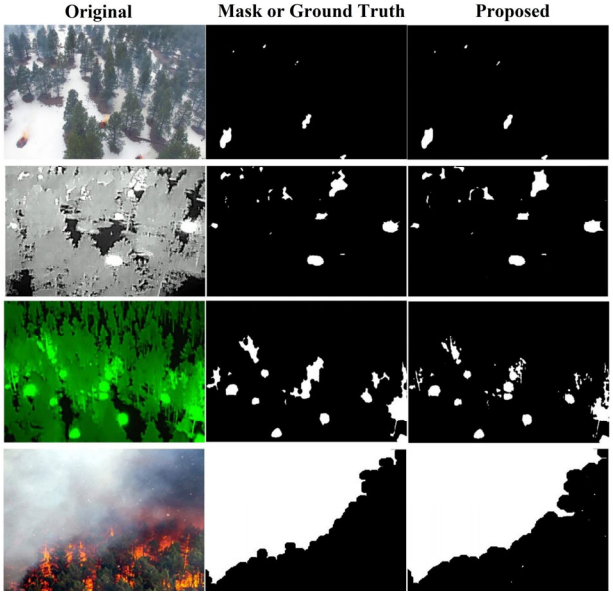


**Fig. 19.** Few test results by proposed methods for fire segmentation and smoke detection and comparing with ground truth data as BW images.

As mentioned in the proposed method section, denoising is part of preprocessing stage and is done by DnCNN algorithm to get rid of any gaussian, impulse noises, or any other pollution in the image which leads to less error and high accuracy for segmentation and classification. Except for PSNR and MSE which are used to compare source and polluted (distorted) images, there are four other metrics that are employed in this research. These metrics are called Image Quality Assessment (IQA) (Wang et al., 2006) metrics. The Structural Similarity Index Measure (SSIM) (Wang et al., 2006) is a proper technique for checking the amount of similarity between two images. The SSIM measure or metric is accessible by comparing local pixel intensity values that is normalized for brightness and contrast elements. Considering f is the original image and g the polluted or distorted one, then SSIM (f, g) is as follow Eq. (16):

$$\mathrm{SSIM} = \left(\frac{2\mu_f\mu_g + C_1}{\mu_f^2 + \mu_g^2 + C_1}\right)^{\alpha}\left(\frac{2\sigma_f\sigma_g + C_2}{\sigma_f^2 + \sigma_y^2 + C_2}\right)^{\beta}\left(\frac{\sigma_{fg} + C_3}{\sigma_f\sigma_g + C_3}\right)^{\gamma} \tag{16}$$

Being $\mu_i$ the average intensity value of the image i, $\sigma_i$ is their SD and $\sigma_{fg}$ is the covariance value for images.

**Table 9**
Parameters of all nature inspired algorithms employed in the experiment

| PARAMETERS | FA Classification | BBO Feature Selection | Bees Segmentation | CSO Contrast Enhancement |
|---|---|---|---|---|
| **Decision Variables (DV)** | Number of Selected Features | Number of All Features (256) | Number of Segments | Lambda, Gamma (Contrast) Values |
| **Decision Variables Size** | [1 DV] | [1 DV] | [1 DV] | [1 DV] |
| **Lower Bound of Variables (LV)** | -5 | 0 | 0 | 0 |
| **Upper Bound of Variables (UP)** | 5 | 1 | 255 | 255 |
| **Iterations** | 200 | 50 | 100 | 100 |
| **Population Size (P)** | 20 | 10 | 20 | 20 |
| **Mutation Rate** | 0.2 | 0.2 | 0.2 | 0.2 |
| **Light Absorption Coefficient** | 1 | - | - | - |
| **Attraction Coefficient** | 2 | - | - | - |
| **Mutation Damping Ratio** | 0.98 | - | - | - |
| **Keep Rate (KR)** | - | 0.2 | - | - |
| **Kept Habitats (KH)** | - | Round (KR*P) | - | - |
| **New Habitats** | - | P-KH | - | - |
| **Emigration Rates (ER)** | - | 0.2 | - | - |
| **Immigration Rates** | - | 1-(ER) | - | - |
| **No of Selected Sites (NSS)** | - | - | 0.5*P | - |
| **No of Selected Elite Sites** | - | - | 0.4*NSS | - |
| **No of Recruited Bees for Selected Sites (NRBS)** | - | - | 0.5*P | - |
| **No of Recruited Bees for Elite Sites** | - | - | 2*NRBS | - |
| **Neighborhood Radius** | - | - | 0.1*(UP-LV) | - |
| **Neighborhood Radius Damp Rate** | - | - | 0.95 | - |
| **Ratio of Rooster** | - | - | - | 0.2 |
| **Ratio of Hen** | - | - | - | 0.6 |
| **Ratio of Hen with Chicks** | - | - | - | 0.3 |

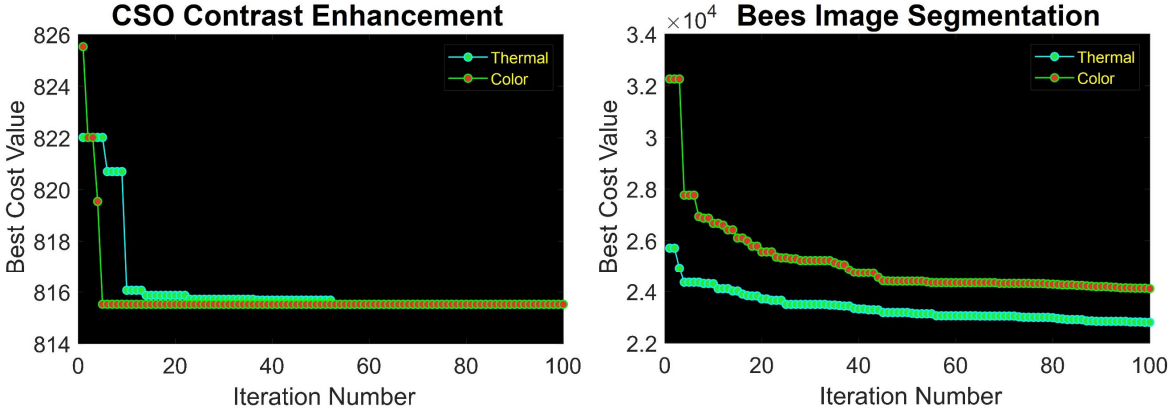


**Fig. 20.** CSO contrast enhancement and Bess image segmentation techniques' performance in 100 iterations on two color and thermal test samples from FLAME dataset

Gradient Conduction Mea n Square Error (GCMSE) (Lopez et al., 2017) is on of the edge-based factors based on MSE. Mostly, GCMSE provides better result than MSE and SSIM. Gradient directions are computed in all four directions by (17) which leads to $G_p$ and acquared results are optimized by the k ratio value:

$$G = \frac{(I_2 - I_1)^2}{(I_2 - I_1)^2 + k^2} \tag{17}$$

The GCMSE is caculated based on Eq. (18):

$$GCMSE = \frac{\sum_{x=1}^{m}\sum_{y=1}^{n}[(I_2(x.y) - I_1(x.y))G_p]^2}{C1 + \sum_{x=1}^{m}\sum_{y=1}^{n} G_p} \tag{18}$$

Edge Based Image Quality Assessment (EBIQA) (Attar et al., 2016) approach acts on the human grasp of the reciving features by eyes. Edges are located and detected by Sobel's edge detector in both images (original and polluted). A pixel window in size of n by n (normally 16 by 16) vectors are made at each image based on Eq. (19) and Eq. (20), where $I_1$ is the original image and $I_2$ is the test image.

$$I_1 = (O.AL.PL.N.VHO) \tag{19}$$

$$I_2 = (O.AL.PL.N.VHO) \tag{20}$$

In Eq. (19) and Eq. (20), 'O' shows orientation of edges image, which is the total number of edges. Also, 'AL' is considered as the length average of all edges. 'PL' will be the total number of pixel values having similar intensity level values. Additionally, 'N' represents the sum of all pixel values, which end up making all edges in image. Finally, 'VH' depicts edges in either vertically or horizontally points as total of pixels of them all. EBIQA is accessible by Eq. (21):

$$EBIQA = \frac{1}{MN}\sum_{i=1}^{M}\sum_{j=1}^{N}\sqrt{(I_1 - I_2)^2} \tag{21}$$

The last metric is Edge-Pixel-based Image Quality Assessment metric (EPIQA) (Mousavi et al., 2022) which extracts the following features for its calculation. In which Edge Density (ED) is the total number of edges in every 8*8 block of the digital image. Edge Length Average (ELA) factor is the Average Length of every block. Edges length values are computed as a decimal number by a simple average. Another factor is called Gray Level Region (GLR) or total number of regions which have same gray level in every block individual. Number of Edge Pixels (NEP) is the number of pixels for each edge in each block. Edge Orientation (EO) factor is number of edges with vertical or horizontal direction in each block. Then, final Euclidean distance of $d_{i,j}$ for two corresponding blocks of original and polluted images, according to Eq. (22). Table 10 shows the average similarity of the dataset's images after denoising by DnCNN by different metrics. For the PSNR average value of 50 means, less noise was available. Also, lower values of MSE indicate less noise in the set of data. The other four factors of GCMSE, EBIQA, and EPIQA should provide higher values to 1 in order to display less pollution or distortion.

$$\begin{aligned} di,j = \Big[\big(ED_{O_{i,j}} - ED_{D_{i,j}}\big)2 + \big(ELAO_{i,j} - ELAD_{i,j}\big)2 + \big(GLRO_{i,j} - GLRD_{i,j}\big)2 + \big(NEPO_{i,j} - NEPD_{i,j}\big)2 \\ + \big(EOO_{i,j} - EOD_{i,j}\big)2\Big]^{(\frac{1}{2})} \end{aligned} \tag{22}$$

And average distance is calculated by final EPIQA Eq. (23) in range of 0-1 plus PSNR of both images.

$$EPIQA = 1 - \left(\frac{1}{M \times N \times MAX(d_{i,j})}\sum_{i=1}^{M}\sum_{j=1}^{N} d_{i,j}\right) + PSNR \tag{23}$$

**Table 10**
Average similarity of dataset images after denoising by DnCNN by various factors

| Dataset | PSNR | MSE | SSIM | GCMSE | EBIQA | EPIQA |
|---|---|---|---|---|---|---|
| **FLAME (Color)** | 48.50 | 0.002 | 0.975 | 0.962 | 0.981 | 0.995 |
| **FLAME (Thermal- White)** | 46.14 | 0.012 | 0.941 | 0.924 | 0.971 | 0.988 |
| **FLAME (Thermal- Green)** | 46.00 | 0.014 | 0.939 | 0.920 | 0.969 | 0.983 |
| **DeepFire (Color)** | 47.32 | 0.006 | 0.960 | 0.954 | 0.979 | 0.990 |

Looking at Table 10, the thermal data of the FLAME dataset had more noise as they had the least resolution and quality. On the other hand, the color data of the FLAME dataset achieved less noise, and DeepFire data was in the middle of the ranking. Fig. 21 shows BBO feature selection performance on all data with 32 selected features out of 256 extracted features by LPQ. LPQ windows size is 29 for all experiments. All parameters are based on Table 9. Fig. 22 depicts 32 selected features for the DeepFire dataset as a box plot alongside related feature indexes out of 256 features. Table 11 represents classification accuracy, precision, recall, and F-measure for train and testing by the Resilient Backpropagation network for

all datasets. Additionally, Table 12 shows the same but the Resilient Backpropagation network's weights and biases are improved by Firefly Algorithm over 200 iterations. All parameters are according to Table 9 for the experiment. Fig. 23 to 26 Receiver Operating Characteristic (ROC) curves (Hanley., 2014), confusion matrixes, and training stages of Firefly algorithm for FLAME and DeepFire datasets after experiments.

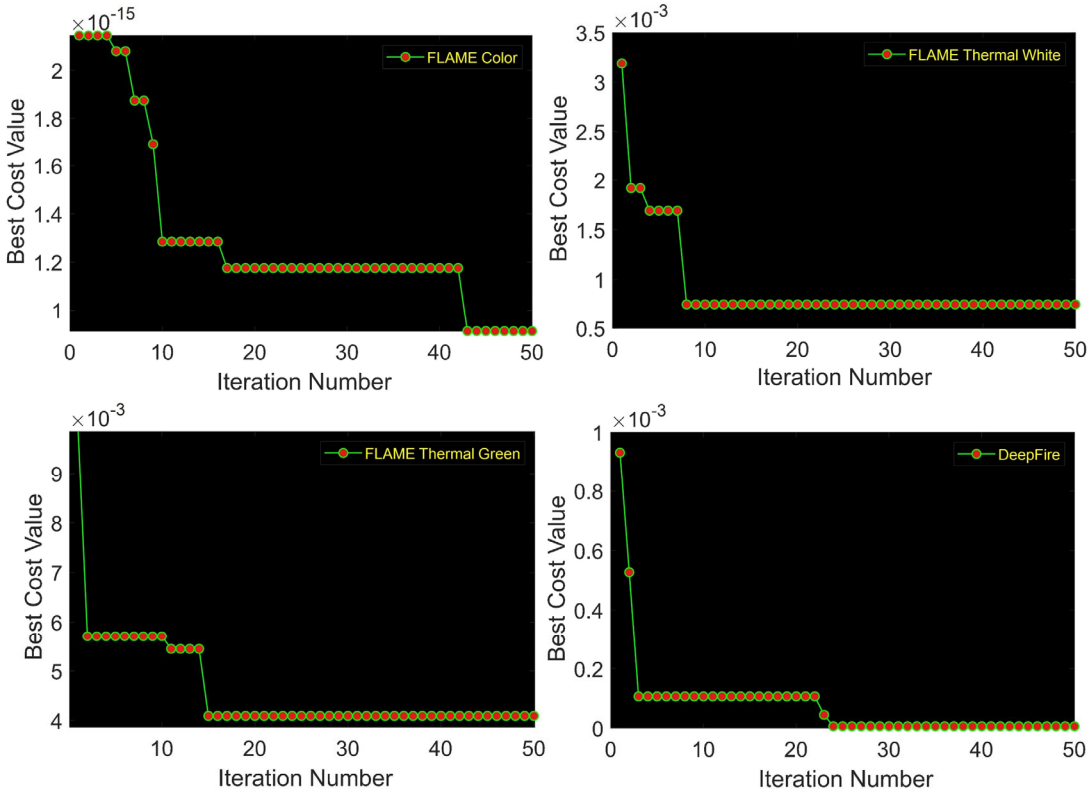


**Fig. 21.** BBO feature selection performance over 50 iterations for all four data (32 features out of 256)

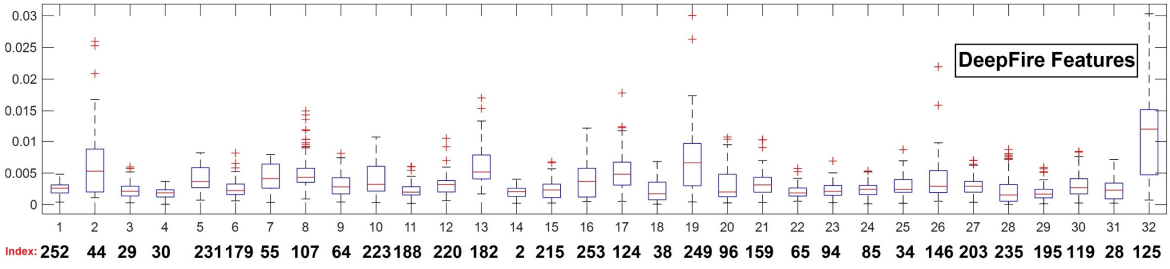


**Fig. 22.** 32 selected features by BBO algorithm for DeepFire dataset as box plot alongside with related features indexes out of 256 features.

**Table 11**
Fire/ no fire classification Accuracy, Precision, Recall, and F-Measure by Resilient Backpropagation network (12 neurons) for all data (80 % train, 20 % test).

| Dataset | Accuracy | Precision | Recall | F-Measure |
|---|---|---|---|---|
| **FLAME (Color)** | Train = 94.32<br>Test = 84.65 | Train = 94.00<br>Test = 86.91 | Train = 93.09<br>Test = 84.73 | Train = 95.70<br>Test = 89.29 |
| **FLAME (Thermal- White)** | Train = 97.11<br>Test = 94.36 | Train = 95.34<br>Test = 95.80 | Train = 97.01<br>Test = 94.00 | Train = 97.53<br>Test = 93.98 |
| **FLAME (Thermal- Green)** | Train = 93.52<br>Test = 89.76 | Train = 96.60<br>Test = 92.17 | Train = 92.95<br>Test = 90.33 | Train = 93.74<br>Test = 91.92 |
| **DeepFire (Color)** | Train = 93.66<br>Test = 90.91 | Train = 95.55<br>Test = 93.28 | Train = 94.69<br>Test = 92.09 | Train = 96.75<br>Test = 94.22 |

**Table 12**
Fire/ no fire classification Accuracy, Precision, Recall, and F-Measure by Improved Resilient Backpropagation network using Firefly Algorithm (12 neurons) for all data (80 % train, 20 % test).

| Dataset | Accuracy | Precision | Recall | F-Measure |
|---|---|---|---|---|
| **FLAME (Color)** | Train = 97.35<br>Test = 91.33 | Train = 97.58<br>Test = 92.83 | Train = 96.80<br>Test = 90.00 | Train = 97.19<br>Test = 91.88 |
| **FLAME (Thermal- White)** | Train = 99.29<br>Test = 96.67 | Train = 99.98<br>Test = 99.97 | Train = 98.41<br>Test = 94.59 | Train = 99.20<br>Test = 97.22 |
| **FLAME (Thermal- Green)** | Train = 96.19<br>Test = 92.40 | Train = 98.65<br>Test = 95.57 | Train = 96.60<br>Test = 93.34 | Train = 98.99<br>Test = 97.91 |
| **DeepFire (Color)** | Train = 97.90<br>Test = 96.88 | Train = 99.61<br>Test = 97.36 | Train = 98.49<br>Test = 96.90 | Train = 99.30<br>Test = 98.61 |

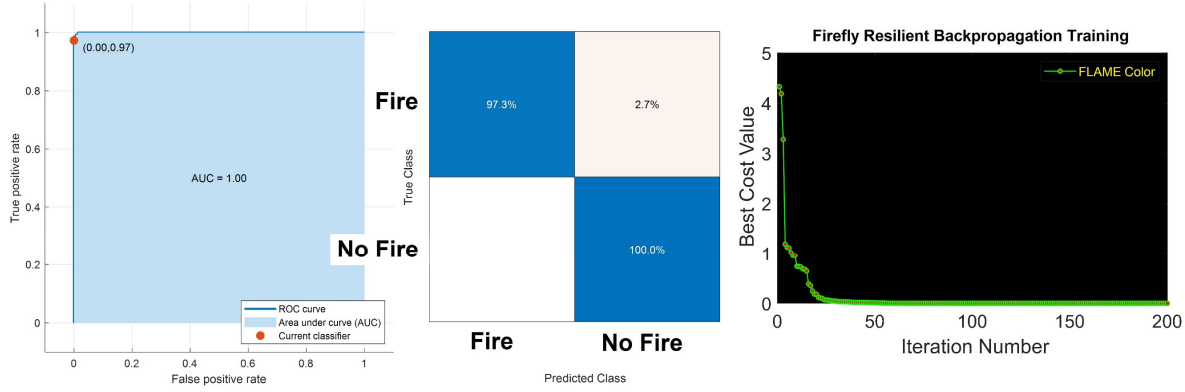


**Fig. 23.** ROC curve, confusion matrix, and FA network training for color data of FLAME dataset

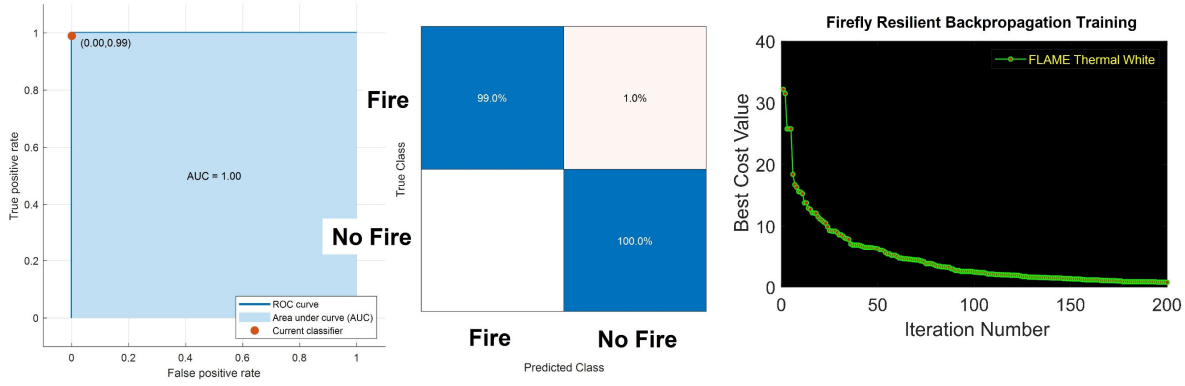


**Fig. 24.** ROC curve, confusion matrix, and FA network training for thermal white data of FLAME dataset

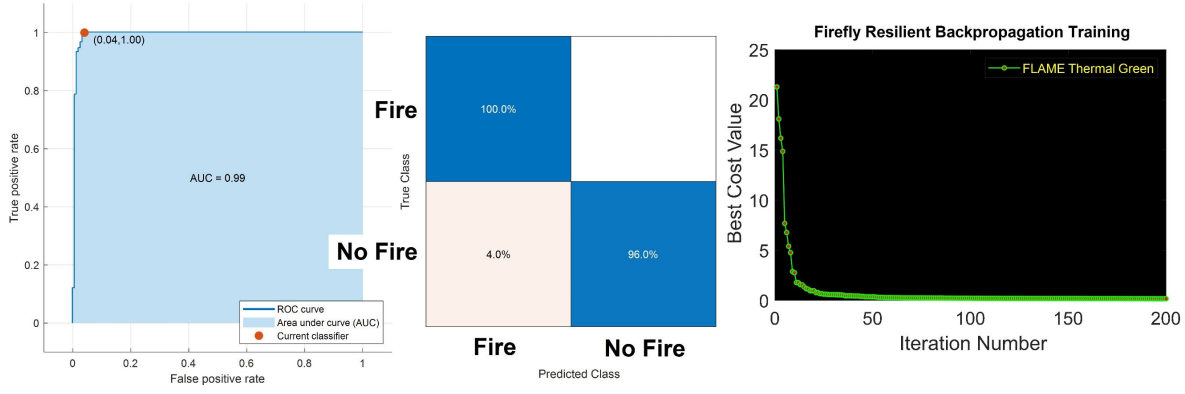


**Fig. 25.** ROC curve, confusion matrix, and FA network training for thermal green data of FLAME dataset

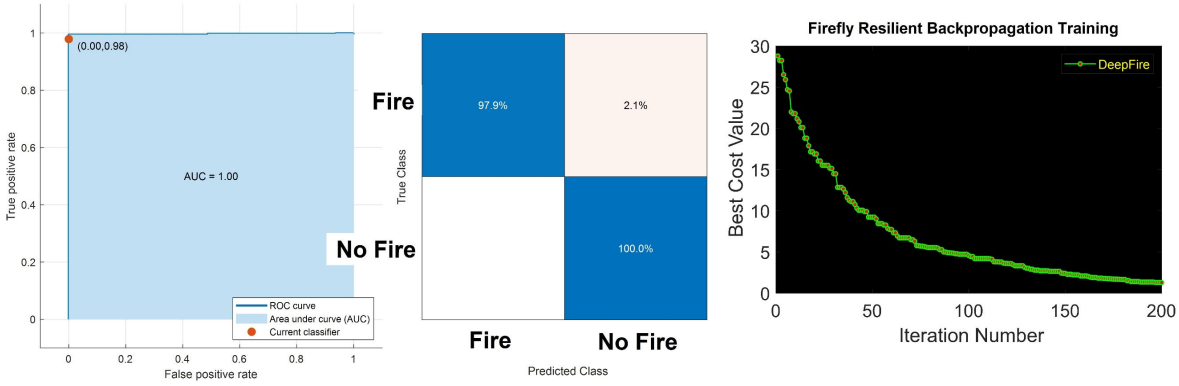


**Fig. 26.** ROC curve, confusion matrix, and FA network training for DeepFire dataset

Looking at Tables 11 and 12, the Resilient Backpropagation network could achieve a proper classification accuracy in train and testing but after weights and biases, improvement by Firefly algorithm recognition accuracy increases by around 5 % which is a success. Also, in the color classification of the FLAME dataset, recognition accuracy improved from 76.23 % by (Shamsoshoara et al., 2021) to 93.33 %. Additionally, the recognition accuracy of the DeepFire dataset improved from 95 % by (khan et al., 2022) to 96.88 % by the proposed system. Tables 13 and 14 present smoke detection results by the proposed method. Fig. 27 depicts the relation between resilient backpropagation and firefly training for two classes of fire and no fire belonging to thermal white (FLAME data) training samples. Fire is considered as class 1 and no fire as class 2 which this figure is showing how two classes are separated, and what errors and outliers are looked like. Other experiments on other data are similar to this figure and this figure is just represented to show the performance of the system on the classification task.

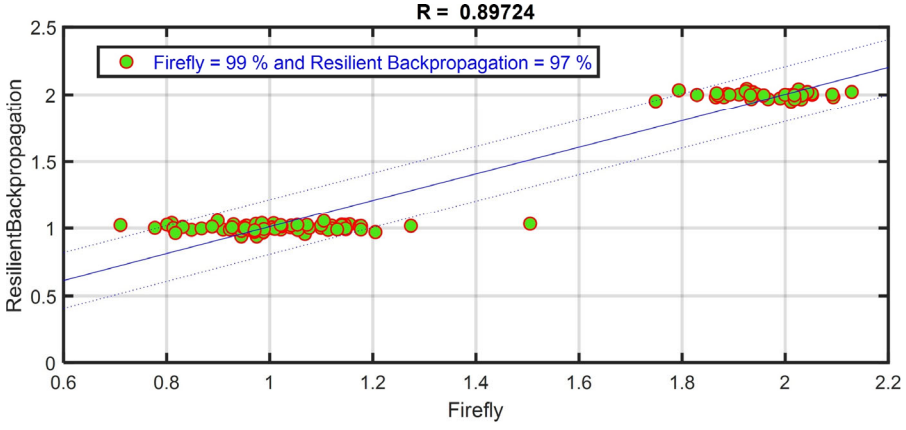


**Fig. 27.** Relation between firefly and resilient backpropagation results on training part of FLAME thermal white data.

**Table 13**
Smoke segmentation results on color data of FLAME dataset

| | Accuracy | Precision | Recall | F1-Measure | IoU | Specificity | MCC | PSNR | MSE |
|---|---|---|---|---|---|---|---|---|---|
| **Proposed** | 85.61 | 83.92 | 86.71 | 85.66 | 86.77 | 86.70 | 87.33 | 31.20 | 0.197 |

**Table 14**
Smoke segmentation results on DeepFire dataset

| | Accuracy | Precision | Recall | F1-Measure | IoU | Specificity | MCC | PSNR | MSE |
|---|---|---|---|---|---|---|---|---|---|
| **Proposed** | 88.92 | 86.74 | 91.39 | 90.55 | 90.00 | 89.61 | 89.75 | 32.65 | 0.166 |

## 4. Conclusion, suggestion and future work

In this research, we present three forest fire or wildfire surveillance methods using computer vision and machine learning techniques in order to fire segmentation, fire classification, and smoke detection which could be employed as firefighter

assistants on UAVs which leads to reducing casualties of civilians and firefighters. Using a nature-inspired algorithm in multiple stages of enhancement, segmentation, feature selection, and classification improved accuracy and outperformed traditional existing methods which were needed as a single life matter, here. Employing multiple pre-processing and learning tasks increases computational time, but as a trained model could be used on UAVs, it is worth sacrificing the time once. The main achievement of this experiment was to improve fire segmentation and fire/ no fire classification accuracy of the most recent methods and dataset of FLAME and DeepFire belonging to 2021 and 2022 years. Researchers FLAME used a deep learning technique and research DeepFire used shallow learning techniques to get their results but proposed hybrid nature-inspired/ shallow learning techniques could outperform them in both segmentation and classification tasks. Fire intensity and fire direction and geometrical calculation were first introduced in this research which could be used on UAVs but needs to be improved and enhanced even more to deal with various types of situations like different angles and distances. DnCNN returned perfect performance for image restoration but it is time-consuming and could be replaced with multiple traditional techniques to remove four main types of noise namely gaussian, impulse, Poisson, and speckle noises which are of future works. Also, adding more performance metrics could increase the clarity of the experiment. Extracting LPQ features were sufficient for the research but feature such as Local Binary Patterns and Gabor Filters as a combination feature could achieve a better result as it covers both spatial and frequency domain. However, time complexity should be considered for this action. The Firefly Algorithm (FA) which is used to improve the weight and biases of resilient backpropagation network act very nicely but the firefly algorithm is a little slower than BBO and BA algorithms and for smaller dataset, it is suggested to use harmony search which is so fast.

## References


Abdi, H., & Williams, L. J. (2010). Principal component analysis. *Wiley interdisciplinary reviews: computational statistics*, *2*(4), 433-459.

Alexandrov, D., Pertseva, E., Berman, I., Pantiukhin, I., & Kapitonov, A. (2019, April). Analysis of machine learning methods for wildfire security monitoring with an unmanned aerial vehicles. In *2019 24th conference of open innovations association (FRUCT)* (pp. 3-9). IEEE.

Almiani, M., Abughazleh, A., Jararweh, Y., & Razaque, A. (2022). Resilient Back Propagation Neural Network Security Model For Containerized Cloud Computing. *Simulation Modelling Practice and Theory*, *118*, 102544.

Attar, A., Shahbahrami, A., & Rad, R. M. (2016). Image quality assessment using edge based features. *Multimedia tools and applications*, *75*(12), 7407-7422.

Barmpoutis, P., Stathaki, T., Dimitropoulos, K., & Grammalidis, N. (2020). Early fire detection based on aerial 360-degree sensors, deep convolution neural networks and exploitation of fire dynamic textures. *Remote Sensing*, *12*(19), 3177.

Benesty, J., Chen, J., Huang, Y., & Cohen, I. (2009). Pearson correlation coefficient. In *Noise reduction in speech processing* (pp. 1-4). Springer, Berlin, Heidelberg.

Bergland, G. D. (1969). A guided tour of the fast Fourier transform. *IEEE spectrum*, *6*(7), 41-52.

Bhawarkar, Y., Bhure, K., Chaudhary, V., & Alte, B. (2022). Diabetic Retinopathy Detection From Fundus Images Using Multi-Tasking Model With EfficientNet B5. In *ITM Web of Conferences* (Vol. 44, p. 03027). EDP Sciences.

Bishop, C. M., & Nasrabadi, N. M. (2006). *Pattern recognition and machine learning* (Vol. 4, No. 4, p. 738). New York: springer.

Bouwmans, T., Javed, S., Sultana, M., & Jung, S. K. (2019). Deep neural network concepts for background subtraction: A systematic review and comparative evaluation. *Neural Networks*, *117*, 8-66.

Bracewell, R. N., & Bracewell, R. N. (1986). *The Fourier transform and its applications* (Vol. 31999, pp. 267-272). New York: McGraw-Hill.

Busin, L., Vandenbroucke, N., & Macaire, L. (2008). Color spaces and image segmentation. *Advances in imaging and electron physics*, *151*(1), 1.

Chandrashekar, G., & Sahin, F. (2014). A survey on feature selection methods. *Computers & Electrical Engineering*, *40*(1), 16-28.

Chen, Y., Zhang, Y., Xin, J., Wang, G., Mu, L., Yi, Y., ... & Liu, D. (2019, June). UAV image-based forest fire detection approach using convolutional neural network. In *2019 14th IEEE conference on industrial electronics and applications (ICIEA)* (pp. 2118-2123). IEEE.

Cruz, H., Eckert, M., Meneses, J., & Martínez, J. F. (2016). Efficient forest fire detection index for application in unmanned aerial systems (UASs). *Sensors*, *16*(6), 893.

Dezfoulian, M. H., MiriNezhad, Y., Mousavi, S. M. H., Mosleh, M. S., & Shalchi, M. M. (2016, September). Optimization of the Ho-Kashyap classification algorithm using appropriate learning samples. In *2016 Eighth International Conference on Information and Knowledge Technology (IKT)* (pp. 167-169). IEEE.

Dhal, K. G., Das, A., Ray, S., Gálvez, J., & Das, S. (2021). Histogram equalization variants as optimization problems: a review. *Archives of Computational Methods in Engineering*, *28*(3), 1471-1496.

Dragaj, V. (2016). Color Image Segmentation Using the Bee Algorithm in the Markovian Framework.

Francies, M. L., Ata, M. M., & Mohamed, M. A. (2022). A robust multiclass 3D object recognition based on modern YOLO deep learning algorithms. *Concurrency and Computation: Practice and Experience*, *34*(1), e6517.

Estrada, M. A. R., & Ndoma, A. (2019). The uses of unmanned aerial vehicles–UAV's-(or drones) in social logistic: Natural disasters response and humanitarian relief aid. *Procedia Computer Science*, *149*, 375-383.

FLIR Vue Pro R, (2022), https://www.flir.co.uk/products/vue-pro-r/?vertical=suas&segment=oem, (Access on 3 July 2022).

Frizzi, S., Bouchouicha, M., Ginoux, J. M., Moreau, E., & Sayadi, M. (2021). Convolutional neural network for smoke and fire semantic segmentation. *IET Image Processing*, *15*(3), 634-647.

Ghali, R., Akhloufi, M. A., & Mseddi, W. S. (2022). Deep learning and transformer approaches for UAV-based wildfire detection and segmentation. *Sensors*, *22*(5), 1977.

Global Forest Watch (GFW), (2022). https://www.globalforestwatch.org/, (Access on 18 Jan 2023).

Gonzalez, R. C. (2009). *Digital image processing*. Pearson education india.

Hanley, J. A. (2014). Receiver operating characteristic (ROC) curves. *Wiley StatsRef: Statistics Reference Online*.

He, K., Zhang, X., Ren, S., & Sun, J. (2016). Deep residual learning for image recognition. In *Proceedings of the IEEE conference on computer vision and pattern recognition* (pp. 770-778).

Hossain, F. A., Zhang, Y. M., & Tonima, M. A. (2020). Forest fire flame and smoke detection from UAV-captured images using fire-specific color features and multi-color space local binary pattern. *Journal of Unmanned Vehicle Systems*, *8*(4), 285-309.

Hossain, S., & Lee, D. J. (2019). Deep learning-based real-time multiple-object detection and tracking from aerial imagery via a flying robot with GPU-based embedded devices. *Sensors*, *19*(15), 3371.

INSPIRE 2, (2022), https://www.dji.com/de/inspire-2, (Access on 3 July 2022).

Jazebi, S., De Leon, F., & Nelson, A. (2019). Review of wildfire management techniques—Part I: Causes, prevention, detection, suppression, and data analytics. *IEEE Transactions on Power Delivery*, *35*(1), 430-439.

Jiao, Z., Zhang, Y., Xin, J., Mu, L., Yi, Y., Liu, H., & Liu, D. (2019, July). A deep learning based forest fire detection approach using UAV and YOLOv3. In *2019 1st International conference on industrial artificial intelligence (IAI)* (pp. 1-5). IEEE.

Jolly, W. M., Cochrane, M. A., Freeborn, P. H., Holden, Z. A., Brown, T. J., Williamson, G. J., & Bowman, D. M. (2015). Climate-induced variations in global wildfire danger from 1979 to 2013. *Nature communications*, *6*(1), 1-11.

Joshi, K., Yadav, R., & Allwadhi, S. (2016, March). PSNR and MSE based investigation of LSB. In *2016 International Conference on Computational Techniques in Information and Communication Technologies (ICCTICT)* (pp. 280-285). IEEE.

Khan, A., Hassan, B., Khan, S., Ahmed, R., & Abuassba, A. (2022). DeepFire: A Novel Dataset and Deep Transfer Learning Benchmark for Forest Fire Detection. *Mobile Information Systems*, *2022*.

Lee, W., Kim, S., Lee, Y. T., Lee, H. W., & Choi, M. (2017, January). Deep neural networks for wild fire detection with unmanned aerial vehicle. In *2017 IEEE international conference on consumer electronics (ICCE)* (pp. 252-253). IEEE.

Lin, Y., Diao, Y., Du, Y., Zhang, J., Li, L., & Liu, P. (2022). Automatic cell counting for phase-contrast microscopic images based on a combination of Otsu and watershed segmentation method. *Microscopy Research and Technique*, *85*(1), 169-180.

López-Randulfe, J., Veiga, C., Rodríguez-Andina, J. J., & Farina, J. (2017, March). A quantitative method for selecting denoising filters, based on a new edge-sensitive metric. In *2017 IEEE International Conference on Industrial Technology (ICIT)* (pp. 974-979). IEEE.

Malhotra, P., Gupta, S., Koundal, D., Zaguia, A., & Enbeyle, W. (2022). Deep Neural Networks for Medical Image Segmentation. *Journal of Healthcare Engineering*, *2022*.

Matthews, B. W. (1975). Comparison of the predicted and observed secondary structure of T4 phage lysozyme. *Biochimica et Biophysica Acta (BBA)-Protein Structure*, *405*(2), 442-451.

Matrice 300 RTK, (2022), *https://www.dji.com/de/matrice-300/specs*, (Access on 3 July 2022).

Martínez-de Dios, J. R., Merino, L., Caballero, F., Ollero, A., & Viegas, D. X. (2006). Experimental results of automatic fire detection and monitoring with UAVs. *Forest Ecology and Management*, *234*(1), S232.

Meng, X., Liu, Y., Gao, X., & Zhang, H. (2014, October). A new bio-inspired algorithm: chicken swarm optimization. In *International conference in swarm intelligence* (pp. 86-94). Springer, Cham.

Misra, D. (2019). Mish: A self regularized non-monotonic neural activation function. *arXiv preprint arXiv:1908.08681*, *4*(2), 10-48550.

Mitchell, T. M., & Mitchell, T. M. (1997). *Machine learning* (Vol. 1, No. 9). New York: McGraw-hill.

Mo, Y., Wu, Y., Yang, X., Liu, F., & Liao, Y. (2022). Review the state-of-the-art technologies of semantic segmentation based on deep learning. *Neurocomputing*, *493*, 626-646.

Mousavi, S. M. H. (2018). A new way to age estimation for rgb-d images, based on a new face detection and extraction method for depth images. *International Journal of Image, Graphics and Signal Processing*, 10(11), 10.

Mousavi, S. M. H., Lyashenko, V., & Prasath, V. B. S. (2019). Analysis of a robust edge detection system in different color spaces using color and depth images. *Computer Optics*, *43*(4), 632-646.

Mousavi, S. M. H., & Kharazi, M. (2017). An edge detection system for polluted images by gaussian, salt and pepper, poisson and speckle noises. In *4th National Conference on Information Technology, Computer & TeleCommunication*.

Mousavi, S., & Mirinezhad, S. (2022). Weevil damage optimization algorithm and its applications. *Journal of Future Sustainability*, 2(4), 133-144.

Mousavi, S. M. H., MiriNezhad, S. Y., & Dezfoulian, M. H. (2017, October). Galaxy gravity optimization (GGO) an algorithm for optimization, inspired by comets life cycle. In *2017 Artificial Intelligence and Signal Processing Conference (AISP)* (pp. 306-315). IEEE.

Mousavi, S. M. H., MiriNezhad, S. Y., & Mirmoini, A. (2017, October). A new support vector finder method, based on triangular calculations and K-means clustering. In *2017 9th International Conference on Information and Knowledge Technology (IKT)* (pp. 46-53). IEEE.

Mousavi, S. M. H., & Mosavi, S. M. H. (2022, March). A New Edge and Pixel-Based Image Quality Assessment Metric for Colour and Depth Images. In *2022 9th Iranian Joint Congress on Fuzzy and Intelligent Systems (CFIS)* (pp. 1-11). IEEE.

National Interagency Fire Center (NIFC), (2022). https://www.nifc.gov/fire-information/nfn, (Access on 3 July 2022).

Nugrahaeni, R. A., & Mutijarsa, K. (2016, August). Comparative analysis of machine learning KNN, SVM, and random forests algorithm for facial expression classification. In *2016 International Seminar on Application for Technology of Information and Communication (ISemantic)* (pp. 163-168). IEEE.

Parrot ANAFI Thermal, (2022), https://www.parrot.com/uk/drones/anafi-thermal, (Access on 3 July 2022).

Pan, S. J., & Yang, Q. (2009). A survey on transfer learning. *IEEE Transactions on knowledge and data engineering*, *22*(10), 1345-1359.

Pham, D. T., Ghanbarzadeh, A., Koç, E., Otri, S., Rahim, S., & Zaidi, M. (2006). The bees algorithm—a novel tool for complex optimisation problems. In *Intelligent production machines and systems* (pp. 454-459). Elsevier Science Ltd.

Phantom 4 Pro V2.0, (2022), https://www.dji.com/de/phantom-4-pro-v2, (Access on 3 July 2022).

Polesel, A., Ramponi, G., & Mathews, V. J. (2000). Image enhancement via adaptive unsharp masking. *IEEE transactions on image processing*, *9*(3), 505-510.

Powers, D. M. (2020). Evaluation: from precision, recall and F-measure to ROC, informedness, markedness and correlation. *arXiv preprint arXiv:2010.16061*.

Rahim, M. A., Azam, M. S., Hossain, N., & Islam, M. R. (2013). Face recognition using local binary patterns (LBP). *Global Journal of Computer Science and Technology*.

Rostami, O., & Kaveh, M. (2021). Optimal feature selection for SAR image classification using biogeography-based optimization (BBO), artificial bee colony (ABC) and support vector machine (SVM): a combined approach of optimization and machine learning. *Computational Geosciences*, *25*(3), 911-930.

Sadeghi, M., Tavakkoli-Moghaddam, R., & Babazadeh, R. (2018). AN EFFICIENT ARTIFICIAL BEE COLONY ALGORITHM FOR A P-HUB COVERING LOCATION PROBLEM WITH TRAVEL TIME RELIABILITY. *International Journal of Industrial Engineering*, *25*(1).

Sazli, M. H. (2006). A brief review of feed-forward neural networks. *Communications Faculty of Sciences University of Ankara Series A2-A3 Physical Sciences and Engineering*, *50*(01).

SCHIEBEL CAMCOPTER, (2022). https://schiebel.net/wp-content/uploads/downloadBrochures/CC_redesign_ENG/index.html#page=10, (Access on 2 July 2022)

Sebe, N., Cohen, I., Garg, A., & Huang, T. S. (2005). *Machine learning in computer vision* (Vol. 29). Springer Science & Business Media.

Setiawan, A. W. (2020, November). Image segmentation metrics in skin lesion: accuracy, sensitivity, specificity, dice coefficient, Jaccard index, and Matthews correlation coefficient. In *2020 International Conference on Computer Engineering, Network, and Intelligent Multimedia (CENIM)* (pp. 97-102). IEEE.

Shamsoshoara, A., Afghah, F., Razi, A., Zheng, L., Fulé, P. Z., & Blasch, E. (2021). Aerial imagery pile burn detection using deep learning: The FLAME dataset. *Computer Networks*, 193, 108001.

Simon, D. (2008). Biogeography-based optimization. *IEEE transactions on evolutionary computation*, *12*(6), 702-713.

Skowronski, M. D., & Harris, J. G. (2006, May). Minimum mean squared error time series classification using an echo state network prediction model. In *2006 IEEE International Symposium on Circuits and Systems* (pp. 4-pp). IEEE.

Smoot, E. E., & Gleason, K. E. (2021). Forest fires reduce snow-water storage and advance the timing of snowmelt across the Western US. *Water*, *13*(24), 3533.

Sun, L., Wang, T., Ding, W., Xu, J., & Lin, Y. (2021). Feature selection using Fisher score and multilabel neighborhood rough sets for multilabel classification. *Information Sciences*, *578*, 887-912.

Srinivas, K., & Dua, M. (2019, August). Fog computing and deep CNN based efficient approach to early forest fire detection with unmanned aerial vehicles. In *International Conference on Inventive Computation Technologies* (pp. 646-652). Springer, Cham.

Tang, Z., Liu, X., Chen, H., Hupy, J., & Yang, B. (2020). Deep learning-based wildfire event object detection from 4K aerial images acquired by UAS. *AI*, *1*(2), 166-179.

Tibshirani, R. (1996). Regression shrinkage and selection via the lasso. *Journal of the Royal Statistical Society: Series B (Methodological)*, *58*(1), 267-288.

Tkalcic, M., & Tasic, J. F. (2003). *Colour spaces: perceptual, historical and applicational background* (Vol. 1, pp. 304-308). IEEE.

Valavanis, K. P., & Vachtsevanos, G. J. (Eds.). (2015). *Handbook of unmanned aerial vehicles* (Vol. 1). Dordrecht: Springer Netherlands.

Vamsidhar, A., Surya Kavitha, T., & Ramesh Babu, G. (2022). Image Enhancement Using Chicken Swarm Optimization. In *Proceedings of the International Conference on Computational Intelligence and Sustainable Technologies* (pp. 555-565). Springer, Singapore.

Wang, S. H., & Zhang, Y. D. (2020). DenseNet-201-based deep neural network with composite learning factor and precomputation for multiple sclerosis classification. *ACM Transactions on Multimedia Computing, Communications, and Applications (TOMM)*, *16*(2s), 1-19.

Wang, Z., & Bovik, A. C. (2006). Modern image quality assessment. *Synthesis Lectures on Image, Video, and Multimedia Processing*, *2*(1), 1-156.

Wang, Z., Wang, E., & Zhu, Y. (2020). Image segmentation evaluation: a survey of methods. *Artificial Intelligence Review*, *53*(8), 5637-5674.

World Health Organization (WHO), (2022). *https://www.who.int/health-topics/wildfires#tab=tab_1* , (Access on 3 July 2022).

Xiao, J., Li, H., & Jin, H. (2022). Transtrack: Online meta-transfer learning and Otsu segmentation enabled wireless gesture tracking. *Pattern Recognition*, *121*, 108157.

Xu, Q., Zhang, C., & Zhang, L. (2015, August). Denoising convolutional neural network. In *2015 IEEE International Conference on Information and Automation* (pp. 1184-1187). IEEE.

Yang, X.-S. (2010). *Nature-inspired metaheuristic algorithms*. Luniver Press

Yuan, B., Cao, H., & Chu, J. (2012, March). Combining local binary pattern and local phase quantization for face recognition. In *2012 International Symposium on Biometrics and Security Technologies* (pp. 51-53). IEEE.

Yuan, C., Liu, Z., & Zhang, Y. (2015, June). UAV-based forest fire detection and tracking using image processing techniques. In *2015 International Conference on Unmanned Aircraft Systems (ICUAS)* (pp. 639-643). IEEE.

Yuan, C., Zhang, Y., & Liu, Z. (2015). A survey on technologies for automatic forest fire monitoring, detection, and fighting using unmanned aerial vehicles and remote sensing techniques. *Canadian journal of forest research*, *45*(7), 783-792.

Yuan, C., Liu, Z., & Zhang, Y. (2019). Learning-based smoke detection for unmanned aerial vehicles applied to forest fire surveillance. *Journal of Intelligent & Robotic Systems*, *93*(1), 337-349.

Zadeh, L. A. (1988). Fuzzy logic. *Computer*, *21*(4), 83-93.

Zang, H., Zhang, S., & Hapeshi, K. (2010). A review of nature-inspired algorithms. *Journal of Bionic Engineering*, *7*(4), S232-S237.

Zenmuse H20N, (2022), https://www.dji.com/de/zenmuse-h20n/specs, (Access on 3 July 2022).

Zhang, K., Zuo, W., Chen, Y., Meng, D., & Zhang, L. (2017). Beyond a gaussian denoiser: Residual learning of deep cnn for image denoising. *IEEE transactions on image processing*, *26*(7), 3142-3155.

Zhang, L., Wang, M., Fu, Y., & Ding, Y. (2022). A Forest Fire Recognition Method Using UAV Images Based on Transfer Learning. *Forests*, *13*(7), 975.

Zhang, H., & Peng, Q. (2022). PSO and K-means-based semantic segmentation toward agricultural products. *Future Generation Computer Systems*, 126, 82-87.